






Improving the Cosmological Constraints by Inferring the Formation Channel of Extreme-mass-ratio Inspirals

LIANG-GUI ZHU (朱良贵) ^{1,*} HUI-MIN FAN (范会敏) ^{2,3,4,5} XIAN CHEN (陈弦) ^{1,6} YI-MING HU (胡一鸣) ^{5,7}
AND JIAN-DONG ZHANG (张建东) ^{5,7}

¹*Kavli Institute for Astronomy and Astrophysics, Peking University, Beijing 100871, People's Republic of China. xian.chen@pku.edu.cn*

²*Department of Physics, College of Physical Science & Technology, Hebei University, Baoding, 071002, People's Republic of China.*

³*Hebei Key Laboratory of High-precision Computation and Application of Quantum Field Theory, Baoding, 071002, People's Republic of China.*

⁴*Hebei Research Center of the Basic Discipline for Computational Physics, Baoding, 071002, People's Republic of China.*

⁵*MOE Key Laboratory of TianQin Mission, TianQin Research Center for Gravitational Physics, Frontiers Science Center for TianQin, CNSA Research Center for Gravitational Waves, Sun Yat-sen University (Zhuhai Campus), Zhuhai 519082, People's Republic of China. fanhm3@mail.sysu.edu.cn, huyiming@mail.sysu.edu.cn*

⁶*Department of Astronomy, School of Physics, Peking University, Beijing 100871, People's Republic of China.*

⁷*School of Physics and Astronomy, Sun Yat-sen University (Zhuhai Campus), Zhuhai 519082, People's Republic of China.*

(Dated: June 5, 2024)

ABSTRACT

Extreme-mass-ratio inspirals (EMRIs) could be detected by space-borne gravitational-wave (GW) detectors, such as the Laser Interferometer Space Antenna (LISA), TianQin and Taiji. Localizing EMRIs by GW detectors can help us select candidate host galaxies, which can be used to infer the cosmic expansion history. In this paper, we demonstrate that the localization information can also be used to infer the formation channel of EMRIs, and hence allow us to extract more precisely the redshift probability distributions. By conducting mock observations of the EMRIs which can be detected by TianQin and LISA, as well as the galaxies which can be provided by the future Chinese Space Station Telescope, we find that TianQin can constrain the Hubble-Lemaître constant H_0 to a precision of $\sim 3\% - 8\%$ and the dark energy equation of state parameter w_0 to $\sim 10\% - 40\%$. The TianQin+LISA network, by increasing the localization accuracy, can improve the precisions of H_0 and w_0 to $\sim 0.4\% - 7\%$ and $\sim 4\% - 20\%$, respectively. Then, considering an illustrative case in which all EMRIs originate in AGNs, and combining the mock EMRI observation with a mock AGN catalog, we show that TianQin can recognize the EMRI-AGN correlation with ~ 1300 detections. The TianQin+LISA network can reduce this required number to ~ 30 . Additionally, we propose a statistical method to directly estimate the fraction of EMRIs produced in AGNs, f_{agn} , and show that observationally deriving this value could significantly improve the constraints on the cosmological parameters. These results demonstrate the potentials of using EMRIs as well as galaxy and AGN surveys to improve the constraints on cosmological parameters and the formation channel of EMRIs.

Keywords: Gravitational waves (678), Black holes (162), Sky surveys (1464), Hubble constant (758), Bayesian statistics (1900), Poisson distribution (1898)

1. INTRODUCTION

The first three observing runs of the Advanced LIGO and Virgo, and KAGRA detectors (LVK) have detected about 90 gravitational-wave (GW) events triggered by the mergers of compact-object binaries (Abbott et al. 2016, 2017a, 2019a, 2021b, 2023a). In addition, evidence

for the existence of GW signal in the nanohertz band is accumulating thanks to the observations of pulsar timing arrays (Agazie et al. 2023; Antoniadis et al. 2023; Reardon et al. 2023; Xu et al. 2023). These observations opened a new era of observational astronomy, in which GW can be used as a new probe of fundamental physics (Abbott et al. 2021c,d), astrophysics (Fishbach & Holz 2017; Abbott et al. 2020b; Fishbach et al. 2021; Abbott et al. 2023b; Bartos et al. 2017; Veronesi et al.

* Boya fellow

2022, 2023), and the cosmic expansion history (Abbott et al. 2017b; Soares-Santos et al. 2019; Fishbach et al. 2019; Hotokezaka et al. 2019; Palmese et al. 2020; Vasylyev & Filippenko 2020; Abbott et al. 2021a; Wang & Giannios 2021; Finke et al. 2021; Abbott et al. 2023c).

The idea of combining a GW event and its electromagnetic (EM) counterpart to establish a “standard siren” to probe the expansion history of the universe, such as measuring the Hubble-Lemaître constant, was first proposed by Schutz (1986). The idea was followed by many later works which gradually established a methodological framework even before the detection of GW (Marković 1993; Holz & Hughes 2005; Dalal et al. 2006; Arun et al. 2009; Petiteau et al. 2011; Babak et al. 2011; Taylor et al. 2012; Del Pozzo 2012; Nisanke et al. 2013). The first successful measurement of the Hubble-Lemaître constant using standard siren was accomplished in 2017 (Abbott et al. 2017b) immediately after the detection of a binary neutron star merger in both GWs (Abbott et al. 2017a) and EM waves (Abbott et al. 2017c). For other GW events, however, a unique EM counterpart is difficult to identify, and hence the redshift should be inferred from the statistical distribution of the galaxies in the same sky area localized by GW detectors (Schutz 1986; MacLeod & Hogan 2008; Petiteau et al. 2011; Del Pozzo 2012). Such “dark sirens” also provide important constraints on the Hubble-Lemaître constant, e.g., in the cases of GW170814 (Soares-Santos et al. 2019) and GW190814 (Palmese et al. 2020; Vasylyev & Filippenko 2020).

So far, using the third Gravitational-wave Transient Catalog (GWTC-3), the LVK collaboration have measured the Hubble-Lemaître constant to a precision of 10% (Abbott et al. 2023c, without using the information from the afterglow of GW170817). Better constraint can be achieved by the next-generation ground-based GW detectors, such as the Advanced LIGO A+/Voyager (Abbott et al. 2020a), Virgo Plus (Acernese et al. 2023), the Einstein Telescope (ET) (Punturo et al. 2010), and Cosmic Explorer (CE) (Reitze et al. 2019). Then we can infer not only the cosmic expansion history, but also the fractional density parameters of the universe and the equation of state (EoS) of the dark energy (Del Pozzo et al. 2017; Cai & Yang 2017; Zhao & Wen 2018; Belgacem et al. 2019; Jin et al. 2020; Yu et al. 2020; You et al. 2021; Chen et al. 2021; Bonilla et al. 2022; Leandro et al. 2022; Song et al. 2022). These measurements will help solve the most difficult questions in today’s cosmology, such as the inconsistency between the measured values of the Hubble-Lemaître constant in the early and late universe (Feeney et al. 2019; Borhanian et al. 2020; Califano et al. 2023; Gupta 2023), which is known as the

“Hubble tension” (Freedman 2017; Aghanim et al. 2020; Riess et al. 2021; Di Valentino et al. 2021; Perivolaropoulos & Skara 2022).

In about a decade, we are likely to have space-borne GW detectors, such as the Laser Interferometer Space Antenna (LISA) (Amaro-Seoane et al. 2017; Colpi et al. 2024), TianQin (Luo et al. 2016; Mei et al. 2021), or Taiji (Hu & Wu 2017). These detectors are sensitive to the GWs in the band of 0.1 mHz – 1 Hz. In this band, the potential GW sources which can be used as standard sirens include stellar-mass ($\sim 10M_{\odot}$) binary black holes (BHs), massive BH (MBH) binaries ($10^5 - 10^8 M_{\odot}$), and extreme-mass-ratio inspirals (EMRIs) (see Auclair et al. 2023, for a review). The usage of the first two sources in cosmology have been extensively studied (Holz & Hughes 2005; Petiteau et al. 2011; Tamanini et al. 2016; Caprini & Tamanini 2016; Del Pozzo et al. 2018; Wang et al. 2022; Wang et al. 2022a; Zhu et al. 2022a,b; Muttoni et al. 2022; Jin et al. 2023). These studies show that the stellar-mass binary BHs detectable by space-borne GW detectors are predominately in the local universe (Sesana 2016; Kyutoku & Seto 2016; Liu et al. 2020), while MBH binaries (MBHBs) are among the loudest GW sources in the milli-Hertz band and hence can be detected to high redshift ($z \gtrsim 10$, Holz & Hughes 2005; Cutler & Vallisneri 2007; Klein et al. 2016; Amaro-Seoane et al. 2017; Wang et al. 2019a).

The third type of low-frequency GW sources which can be used as standard sirens are EMRIs. EMRI normally resides at the center of a galaxy and consists of an MBH and an inspiralling stellar-mass BH (Amaro-Seoane 2018). The potential of using LISA EMRIs to study cosmology was first pointed out in MacLeod & Hogan (2008), and later studied in more detail in Laghi et al. (2021); Liu et al. (2023). These earlier studies considered only the EMRIs with $z < 1$ where the galaxy catalogs are relatively more complete. However, population studies have shown that space-borne GW detectors can catch EMRIs up to $z \approx 3$ or higher (Babak et al. 2017; Fan et al. 2020; Bonetti & Sesana 2020). At such high redshifts, although the current galaxy catalog is incomplete, future space telescopes will be able to conduct a more complete survey of the galaxies (Gong et al. 2019; Ivezić et al. 2019; Scaramella et al. 2022). In addition, besides LISA, other space-borne GW detectors, such as TianQin and Taiji, can also detect EMRIs. A joint observation by multiple detectors in principle can improve the sky localization of a GW source by orders of magnitude (Ruan et al. 2020; Gong et al. 2021). These observational prospects in general should improve the constraint on cosmological parameters by EMRIs.

The prospect of using EMRIs to constrain the cosmological parameters relies on not only the completeness of a galaxy catalog, but also the accuracy of the redshift which can be inferred from the galaxy catalog. When extracting the redshift probability distributions of EMRIs from galaxy catalogs, previous works (MacLeod & Hogan 2008; Laghi et al. 2021; Liu et al. 2023) have assumed that all galaxies have an equal probability to host an EMRI. However, there might exist a substantial bias towards specific types of galaxies in the formation of EMRIs, as alternative formation channels could potentially yield higher EMRI rates in comparison to the standard channel (Hopman & Alexander 2005; Babak et al. 2017; Amaro-Seoane 2018). These alternative channels include binary separations (Miller et al. 2005), MBHB systems (Mazzolari et al. 2022; Naoz et al. 2022; Naoz & Haiman 2023) and AGNs (Levin 2003, 2007; Yunes et al. 2011; Pan & Yang 2021; Pan et al. 2021; Derdzinski & Mayer 2023). In particular, AGNs are potentially favourable environments for forming EMRIs because the accretion disks of AGNs can capture more stellar-mass BHs and BH binaries and drive them to migrate towards the central MBHs than normal galactic nuclei can do (Tagawa et al. 2020; Abbott et al. 2023b). The major properties predicted by the different EMRI formation channels, such as the EMRI rates, eccentricities at plunges, and masses of the MBHs and stellar-mass BHs, are subject to considerable uncertainties, posing challenges in determining the origins of EMRIs. Therefore, what type of galaxies in a catalog can be considered as the hosts of EMRIs remains a question.

Recently, a statistical framework has been proposed which allows one to test the spatial correlation between GW sources and AGNs even in the absence of identifying the host galaxies of the GW sources (Bartos et al. 2017). The framework utilizes a Poisson distribution to describe the likelihood of the number of candidate host AGNs for the GW source, and constrains the spatial correlation between the GW sources and AGNs by a likelihood-ratio-based method. Several works have demonstrated the effectiveness of this framework in identifying the host galaxies of the LVK binary BHs (Veronesi et al. 2022, 2023) or the MBHBs of future space-borne GW detectors (Zhu & Chen 2024). Such a method in principle can be used to infer the fraction of EMRIs which originate in AGNs. Knowing this fraction will help us better weigh the large number of candidate host galaxies in the sky area localized for an EMRI, so that we can more precisely extract the redshift probability distributions and measure cosmological parameters.

Therefore, in this work we will apply the aforementioned statistical framework to EMRIs, and study its ef-

fectiveness in constraining the cosmological parameters and testing the spatial correlation between EMRIs and AGNs. To facilitate the study, we consider TianQin, as well as a network composed of TianQin and LISA, as the future observational instruments. This paper is organized as follows. In Section 2 we introduce the statistical analysis framework that we use to infer the cosmic expansion history and test the EMRI-AGN correlation. In Section 3 we conduct mock observations. The results are shown in Section 4 for the cosmological prospects and Section 5 for the prospects of inferring the EMRI-AGN correlation. In Section 6, we discuss some of the factors that can affect the results. Finally, in Section 7 we summarize the main findings of this work and the implications of our results.

2. METHODOLOGY

2.1. Cosmological model

We assume that the universe is flat (Aghanim et al. 2020; Dhawan et al. 2021) and can be described by the Friedmann-Lemaître-Robertson-Walker metric. From the Friedmann equations, the expansion rate of the universe can be described by

$$H(z) = H_0 \sqrt{\Omega_M(1+z)^3 + \Omega_\Lambda \exp\left[3 \int_0^z \frac{1+w(z')}{1+z'} dz'\right]}, \quad (1)$$

where $H(z)$ is called as the Hubble-Lemaître parameter and $H_0 \equiv H(z=0)$ is its current value, Ω_M and Ω_Λ are respectively the ratios of the total matter density and dark energy density to the critical density of the universe (they satisfy $\Omega_M + \Omega_\Lambda = 1$ in a flat-universe), and $w(z)$ describes the dark energy EoS as a function of redshift z .

In this work, we consider two dark energy models, namely the standard model—the cosmological constant Λ , and the Chevallier-Polarski-Linder (CPL) model (Chevallier & Polarski 2001; Linder 2003). (i) For the cosmological constant model, the EoS of the dark energy is constantly equal to minus one, i.e., $w(z) \equiv -1$. This model, together with the cold dark matter model and the spatially-flat assumption, constitute the so-called standard cosmological model—flat- Λ CDM. (ii) For the CPL model, the EoS of the dark energy is modeled as a function of $w(z) = w_0 + w_a z/(1+z)$ (Chevallier & Polarski 2001), where w_0 and w_a are two extra parameters. The analytic expression of Equation (1) is $H(z) = H_0 \sqrt{\Omega_M(1+z)^3 + \Omega_\Lambda(1+z)^{3(1+w_0+w_a)} \exp\left(-\frac{3w_a z}{1+z}\right)}$. In particular, when $w_0 = -1$ and $w_a = 0$, the CPL model recovers the cosmological constant model.

Regardless of dark energy models, we have the “luminosity distance–redshift” ($D_L - z$) relation under a flat-universe according to the expansion effect of the universe, i.e.,

$$D_L = c(1+z) \int_0^z \frac{1}{H(z')} dz', \quad (2)$$

where c is the speed of light. In our simulations, we fix the cosmological parameters to the values: $H_0 \equiv h \times 100 \text{ km s}^{-1} \text{ Mpc}^{-1} = 67.8 \text{ km s}^{-1} \text{ Mpc}^{-1}$ (here h is the dimensionless Hubble-Lemaître constant), $\Omega_M = 0.307$, $w_0 = -1$, and $w_a = 0$.

2.2. Bayesian framework for GW cosmology

To constrain the cosmological parameters by combining the GW and EM data, we adopt the Bayesian framework presented in Chen et al. (2018). However the estimation of the completeness of the galaxy catalog is modified. Here the estimation is based on the correlation between the MBHs in EMRIs and their host galaxies. More specifically, we use the approximate linear relationship between the masses of MBHs and the (bulge) luminosities of the galaxies (which is known as the $M_{\text{MBH}} - L$ relation; Ferrarese & Merritt 2000; Scott & Graham 2013; Kormendy & Ho 2013).

Given a GW data set composed of N independent GW events $\mathcal{D}^{\text{gw}} \equiv \{d_1^{\text{gw}}, d_2^{\text{gw}}, \dots, d_i^{\text{gw}}, \dots, d_N^{\text{gw}}\}$ as well as the corresponding data set of EM counterparts $\mathcal{D}^{\text{em}} \equiv \{d_1^{\text{em}}, d_2^{\text{em}}, \dots, d_i^{\text{em}}, \dots, d_N^{\text{em}}\}$, the *posterior* probability distribution of the cosmological parameters (denote as $\Omega \equiv \{H_0, \Omega_M, w_0, w_a\}$) that we are interested in can be expressed as

$$p(\Omega | \mathcal{D}^{\text{gw}}, \mathcal{D}^{\text{em}}, I) \propto p_0(\Omega | I) p(\mathcal{D}^{\text{gw}}, \mathcal{D}^{\text{em}} | \Omega, I) \propto p_0(\Omega | I) \prod_i p(d_i^{\text{gw}}, d_i^{\text{em}} | \Omega, I), \quad (3)$$

where I indicates all the relevant additional information, $p_0(\Omega | I)$ is the *prior* probability distribution for Ω , and $p(d_i^{\text{gw}}, d_i^{\text{em}} | \Omega, I)$ represents the *likelihood* of observing the i th GW event as well as the corresponding EM signal. Because the data contain noise such that different sources with different right ascensions α and declinations δ , luminosity distances D_L , redshifts z , masses M , and luminosities L may generate the same observational data. Therefore, the likelihood needs to marginalize all possible $(\alpha, \delta, D_L, z, M, L)$, i.e.,

$$p(d_i^{\text{gw}}, d_i^{\text{em}} | \Omega, I) = \frac{\int p(d_i^{\text{gw}}, d_i^{\text{em}}, \alpha, \delta, D_L, z, M, L | \Omega, I) d\alpha d\delta dD_L dz dM dL}{\beta(\Omega | I)}, \quad (4)$$

where $\beta(\Omega | I)$ is a normalization factor accounting for the selection effects in GW and EM observations (Mandel et al. 2019; Chen et al. 2018; Soares-Santos et al. 2019).

To calculate the numerator in Equation (4), we separate $p(d_i^{\text{gw}}, d_i^{\text{em}}, \alpha, \delta, D_L, z, M, L | \Omega, I)$ into

$$\begin{aligned} & p(d_i^{\text{gw}}, d_i^{\text{em}}, \alpha, \delta, D_L, z, M, L | \Omega, I) \\ &= p(d_i^{\text{gw}}, d_i^{\text{em}} | \alpha, \delta, D_L, z, M, L, \Omega, I) \\ & \quad \times p_0(\alpha, \delta, D_L, z, M, L | \Omega, I) \\ &= p(d_i^{\text{gw}} | \alpha, \delta, D_L, M, \Omega, I) p(d_i^{\text{em}} | \alpha, \delta, z, L, \Omega, I) \\ & \quad \times p_0(D_L | z, \Omega, I) p_0(M | z, L, \Omega, I) p_0(\alpha, \delta, z, L | \Omega, I). \end{aligned} \quad (5)$$

The term $p(d_i^{\text{gw}} | \alpha, \delta, D_L, M, \Omega, I)$ is the likelihood of the GW data (Finn 1992; Sathyaprakash & Schutz 2009) after marginalized over all other parameters that are unrelated to the cosmic expansion history, and $p(d_i^{\text{em}} | \alpha, \delta, z, L, \Omega, I)$ is the likelihood of the corresponding EM data. For dark sirens, because there is no information from the observations of the EM counterparts, we can define d_i^{em} to null, as well as define the likelihood $p(d_i^{\text{em}} | \alpha, \delta, z, L, \Omega, I)$ to constant (Chen et al. 2018). The term $p_0(D_L | z, \Omega, I)$ is a Dirac delta function, i.e., $p_0(D_L | z, \Omega, I) = \delta_D(D_L - \hat{D}_L(z, \Omega))$ (here $\hat{D}_L(z, \Omega)$ represents Equation (2)), because D_L is a function of z given a cosmology.

The term $p_0(M | z, L, \Omega, I)$ can be approximated as a uniform distribution of M , i.e.,

$$p_0(M | z, L, \Omega, I) \propto \mathcal{U}[(1+z)(\hat{M}(L) - 3\sigma_M), (1+z)(\hat{M}(L) + 2\sigma_M)](M), \quad (6)$$

where the two values in square bracket $\mathcal{U}[\dots, \dots]$ represent the lower and upper boundaries of the uniform distribution, $\hat{M}(L)$ represents the mass of the MBH as a function of the luminosity of the host galaxy, and σ_M is the standard deviation. The expression of $p_0(M | z, L, \Omega, I)$ holds just for EMRI (and MBHB) GW sources due to the $M_{\text{MBH}} - L$ relation. The reason for adopting a uniform rather than a Gaussian distribution is that the data for which the $M_{\text{MBH}} - L$ relation is derived have many outliers (Ferrarese & Merritt 2000; Scott & Graham 2013; Kormendy & Ho 2013). The function $\hat{M}(L)$ can be written as

$$\lg\left(\frac{\hat{M}(L)}{M_\odot}\right) \approx a_{\text{fit}} + b_{\text{fit}} \left[M_\odot^* - 2.5 \lg\left(\frac{L}{L_\odot}\right) + 23.4 \right], \quad (7)$$

(Scott & Graham 2013), where a_{fit} and b_{fit} are the fitting zeropoint and slope, and $M_\odot = 1.989 \times 10^{30} \text{ kg}$, $M_\odot^* = +4.8 \text{ mag}$ and $L_\odot = 3.8 \times 10^{33} \text{ erg s}^{-1}$ are the mass,

absolute magnitude, and luminosity of the Sun, respectively. The best-fitting parameters for Equation (7) in the K -band are $a_{\text{fit}} = 8.04$ and $b_{\text{fit}} = -0.48$ with a root-mean-square scatter of $\sigma_M = 0.4$ in $\lg(M/M_\odot)$ (Scott & Graham 2013). Notice that the uniform distribution adopted by us is not symmetric around $\hat{M}(L)$ because there is a fraction of galaxies with lighter MBHs compared to the predicted $\hat{M}(L)$ (Jiang et al. 2011; Scott & Graham 2013; Kormendy & Ho 2013).

The last term $p_0(\alpha, \delta, z, L|\mathbf{\Omega}, I)$ in Equation (5) is a prior distribution for the spatial positions and luminosities of galaxies. To get a proper prior, we adopt the standard assumption that the spatial probability distribution of GW sources is proportional to the number density of galaxies (Schutz 1986; MacLeod & Hogan 2008; Petiteau et al. 2011; Del Pozzo 2012; Chen et al. 2018; Fishbach et al. 2019; Soares-Santos et al. 2019; Gray et al. 2020; Finke et al. 2021; Abbott et al. 2023c). Further taking into account the selection effect that many galaxies are too dim to be recorded by surveys, we can express the prior as

$$p_0(\alpha, \delta, z, L|\mathbf{\Omega}, I) = f_{\text{compl}} p_{\text{obs}}(\alpha, \delta, z, L|\mathbf{\Omega}, I) + (1 - f_{\text{compl}}) p_{\text{miss}}(\alpha, \delta, z, L|\mathbf{\Omega}, I), \quad (8)$$

where $p_{\text{obs}}(\alpha, \delta, z, L|\mathbf{\Omega}, I)$ represents a distribution function of observed galaxies from EM surveys, f_{compl} is the completeness fraction of the observed galaxy catalog, and $p_{\text{miss}}(\alpha, \delta, z, L|\mathbf{\Omega}, I)$ represents the probability distribution function (PDF) of the unobservable galaxies.

To calculate $p_0(\alpha, \delta, z, L|\mathbf{\Omega}, I)$, we need specific expressions for the two terms on the right-hand side of Equation (8). (i) The distribution function of observed galaxies $p_{\text{obs}}(\alpha, \delta, z, L|\mathbf{\Omega}, I)$ can generally be written as

$$p_{\text{obs}}(\alpha, \delta, z, L|\mathbf{\Omega}, I) \propto \sum_{j=1}^{N_{\text{gal}}} \left[\delta_{\text{D}}(\alpha - \alpha_j) \delta_{\text{D}}(\delta - \delta_j) \times \mathcal{N}[\bar{z}_j, \sigma_{z;j}](z) \mathcal{N}[\bar{L}_j, \sigma_{L;j}](L) \right], \quad (9)$$

where N_{gal} is the total number of the observed galaxies and two $\mathcal{N}[\bar{x}, \sigma_x](x)$ represent Gaussian distributions of x with mean values \bar{x} and standard deviations σ_x . Here, because the errors of sky positions of galaxies in EM surveys are much smaller than the sky localization errors of the GW sources, the distribution of (α, δ) of galaxies can be approximately expressed as two Dirac delta functions. (ii) For the unobservable galaxies, their PDF can be expressed as

$$p_{\text{miss}}(\alpha, \delta, z, L|\mathbf{\Omega}, I) \propto \text{erfc}(L) \Phi(L, z) \frac{dV_c}{dz d\hat{\Omega}}, \quad (10)$$

where

$$\text{erfc}(L) = \frac{1}{\sqrt{2\pi\bar{\sigma}_L^2}} \int_L^\infty \exp\left[-\frac{(L' - \hat{L}_{\text{thr}}(z, \mathbf{\Omega}))^2}{2\bar{\sigma}_L^2}\right] dL'$$

is the complementary error function with mean value $\hat{L}_{\text{thr}}(z, \mathbf{\Omega})$ and standard distribution $\bar{\sigma}_L$, $\Phi(L, z)$ represents the luminosity function of the galaxies at z (Schechter 1976; Dahlen et al. 2005; Marchesini et al. 2007), V_c is the comoving volume, and $d\hat{\Omega} = \cos\delta d\alpha d\delta$ represents the differential solid angle. The mean value $\hat{L}_{\text{thr}}(z, \mathbf{\Omega})$ is a luminosity threshold for an observable galaxy with z in a cosmology $\mathbf{\Omega}$, and it depends on the limiting magnitude m_{limit}^* of the galaxy survey. We can calculate it with

$$\lg\left(\frac{\hat{L}_{\text{thr}}(z, \mathbf{\Omega})}{L_\odot}\right) = \frac{1}{2.5} \left[M_\odot^* - m_{\text{limit}}^* + 5 \lg\left(\frac{\hat{D}_L(z, \mathbf{\Omega})}{1 \text{ Mpc}}\right) + 25 \right]. \quad (11)$$

The complete expression of $p_0(\alpha, \delta, z, L|\mathbf{\Omega}, I)$ additionally requires a reasonable estimation for the completeness of the observed galaxy catalog. In this work, we consider the role of the $M_{\text{MBH}} - L$ relation for estimating the completeness of galaxy catalogs. We assume that the completeness depends not only on the galaxy catalog itself, but also on the property of the EMRI source (such as the mass of the MBH). The completeness fraction can be estimated by

$$f_{\text{compl}} \approx 1 - \left[\int p(d_i^{\text{gw}}|\alpha, \delta, D_L, M, \mathbf{\Omega}, I) p_0(D_L|z, \mathbf{\Omega}, I) \times p_0(M|z, L, \mathbf{\Omega}, I) \times p_{\text{miss}}(\alpha, \delta, z, L|\mathbf{\Omega}, I) d\alpha d\delta dD_L dM dz dL \right]. \quad (12)$$

The $M_{\text{MBH}} - L$ relation is the statistical basis that enables the term $p_0(M|z, L, \mathbf{\Omega}, I)$ to connect the EMRI GW source to the galaxy catalog. From Equation (12), we can find that for an EMRI source with a more massive MBH, the completeness of the same galaxy catalog is higher.

Finally, to calculate the denominator $\beta(\mathbf{\Omega}|I)$ in Equation (4), we adopt the same estimated approach as presented in Chen et al. (2018) (also see Gray et al. 2020; Finke et al. 2021; Abbott et al. 2023c; Zhu & Chen 2023). For dark sirens, the denominator is determined by the GW data d^{gw} and the prior $p_0(\alpha, \delta, z, L|\mathbf{\Omega}, I)$, and we have

$$\beta(\mathbf{\Omega}|I) = \int_{\text{detectable}} p(d^{\text{gw}}|\hat{D}_L(z, \mathbf{\Omega}), M, I) p_0(M|z, L, \mathbf{\Omega}, I) \times p_0(\alpha, \delta, z, L|\mathbf{\Omega}, I) dd^{\text{gw}} d\alpha d\delta dM dz. \quad (13)$$

Here, the equation represents an integration over the possible GW data d^{gw} that the signal-to-noise ratio (SNR) is greater than the detection threshold.

2.3. Statistical framework for constraining the formation channel of EMRIs

An effective constraint on the formation channel of EMRIs can be obtained by testing the spatial correlation between EMRIs and AGNs. We set the null hypothesis of our test to be that EMRIs can reside in either normal galaxies or AGNs. It means that the probability that a detected EMRI originates in an AGN is proportional to the fraction of AGNs among all galaxies. Our alternative hypothesis is that EMRIs predominantly reside in AGNs.

To statistically test our null hypothesis, we use the same statistical framework presented in [Zhu & Chen \(2024\)](#), which was developed upon the work of ([Bartos et al. 2017](#), also see earlier [Braun et al. \(2008\)](#)) and modified to test the spatial correlation between MBHB mergers and AGNs. Given that the spatial number density of AGNs is ρ_{agn} , and the spatial localization error volume of the i th detected EMRI is ΔV_i , in the null hypothesis the number $N_{\text{agn},i}$ of AGNs within the error volume ΔV_i will follow a Poisson distribution with an expectation of $\rho_{\text{agn}}\Delta V_i$, i.e.,

$$B_i(N_{\text{agn},i}) = \text{Poisson}(N_{\text{agn},i}, \rho_{\text{agn}}\Delta V_i). \quad (14)$$

In the alternative hypothesis, there is one guaranteed host AGN within ΔV_i . Therefore, the number of the rest non-host AGNs, $N_{\text{agn},i} - 1$, will follow the Poisson distribution with the expectation $\rho_{\text{agn}}\Delta V_i$, i.e.,

$$S_i(N_{\text{agn},i}) = \text{Poisson}(N_{\text{agn},i} - 1, \rho_{\text{agn}}\Delta V_i). \quad (15)$$

Taking into account our lack of knowledge about the formation channel of EMRIs, we assume that a fraction f_{agn} of detected EMRIs are from AGNs, while the rest detected EMRIs originate in normal galaxies. Effectively, it means that the probability that an individual EMRI originates in an AGN is equal to f_{agn} . Furthermore, taking into account the incompleteness of the AGN catalog, we can write the individual likelihood of the i th detected EMRI as

$$\mathcal{L}_i(f_{\text{agn}}) = f_{\text{agn}}f_{\text{compl},i}^{\text{agn}}S_i + (1 - f_{\text{agn}}f_{\text{compl},i}^{\text{agn}})B_i \quad (16)$$

([Zhu & Chen 2024](#)), where $f_{\text{compl},i}^{\text{agn}}$ represents the completeness fraction of the AGN catalog when the i th detected EMRI is evaluated. For the estimation of $f_{\text{compl},i}^{\text{agn}}$, we follow exactly the approach of [Zhu & Chen \(2024\)](#), by considering the correlation between the luminosities

of AGNs and the masses of their central MBHs. For a GW catalog composed of N EMRIs, the total likelihood can be expressed as

$$\mathcal{L}(f_{\text{agn}}) = \prod_i \mathcal{L}_i(f_{\text{agn}}). \quad (17)$$

Several factors render it exceedingly challenging to accurately infer f_{agn} directly from Equation (17), including (i) the degeneracy between f_{agn} and $f_{\text{compl},i}^{\text{agn}}$, (ii) the sensitivity of the likelihood to the accurate determination of ρ_{agn} , and (iii) the data $\{N_{\text{agn},i}\}$ of the likelihood is not directly related to f_{agn} . Regarding (i) and (ii), accurate estimations of both $f_{\text{compl},i}^{\text{agn}}$ and ρ_{agn} are impeded by selection effects. For (iii), Because the number N_{agn} of candidate host AGNs is proportional to the spatial localization error volume of the EMRI, not by correlation with f_{agn} . An EMRI originated in an AGN merely implies an anticipated increase of one in the count of candidate host AGNs for this EMRI, compared to a random scenario.

To statistically constrain the fraction f_{agn} in Equation (17), we follow [Braun et al. \(2008\)](#) and [Bartos et al. \(2017\)](#) to introduce a likelihood ratio

$$\lambda = 2 \ln \left[\frac{\mathcal{L}(f_{\text{agn}})}{\mathcal{L}(0)} \right]. \quad (18)$$

In the null hypothesis, in which the value of f_{agn} equals to the fraction of AGNs among all galaxies in the universe, the likelihood ratio λ is governed by the random fluctuation of the spatial number density of AGNs, and will follow a ‘‘background distribution’’ $P_{\text{bg}}(\lambda)$. Conversely, in the alternative hypothesis that f_{agn} significantly exceeds the fraction of AGNs among all galaxies, λ becomes governed by the spatial correlation between EMRIs and AGNs. This is because, under this condition, the likelihoods $\mathcal{L}(f_{\text{agn}})$ and $\mathcal{L}(0)$ in Equation (18) exhibit significant discrepancies. For illustrative purposes, the distributions of the likelihood ratio λ in the null and alternative hypotheses, as well as their variation with f_{agn} , are presented in Appendix A. A very important property is that the λ derived from real observation of EMRIs will deviate more from $P_{\text{bg}}(\lambda)$ when the fraction of the EMRIs originate in AGNs is larger. In the analysis, $P_{\text{bg}}(\lambda)$ can be determined by Monte-Carlo simulations, and the deviation of the median λ relative to $P_{\text{bg}}(\lambda)$ can be quantified by an p -value. If this p -value becomes less than 0.00135, we can claim that we can reject the null hypothesis with a significance of 3σ , i.e., confirm the spatial correlation between the EMRIs and AGNs.

Finally, we estimate the uncertainty in the observational constraint on f_{agn} . We denote the likelihood ratio

derived from observational data (the numbers of candidate host AGNs of the detected EMRIs) as $\lambda_s(f_{\text{agn}})$, where the subscript “s” stands for “signal”. Notice that its value varies with the underlying AGN fraction f_{agn} . To check whether $\lambda_s(f_{\text{agn}})$ is consistent with or can be rejected by the background distribution of λ , we introduce an integrated probability

$$CDF(\lambda_s, f_{\text{agn}}) = \frac{1}{\mathcal{N}} \int_{\lambda_s(f_{\text{agn}})}^{\infty} P(\lambda|f_{\text{agn}}) d\lambda, \quad (19)$$

where $P(\lambda|f_{\text{agn}})$ is the conditional PDF of the likelihood ratio λ given f_{agn} , and \mathcal{N} is a normalization factor. In our simulations, each $P(\lambda|f_{\text{agn}})$ is derived from about 10^4 independent Monte-Carlo simulations.

The meanings of $\lambda_s(f_{\text{agn}})$ and $P(\lambda|f_{\text{agn}})$ are illustrated in Figure 1. It shows that the conditional PDF $P(\lambda|0.1)$ (black dotted curve) is clearly inconsistent with the observed value of λ_s , because $CDF(\lambda_s, 0.1)$ is small. As f_{agn} increases, the PDF $P(\lambda|f_{\text{agn}})$ shifts towards larger values of λ , and becomes more consistent with λ_s . Therefore, we estimate the error of f_{agn} through the following steps. (i) We increase f_{agn} until we find a value which satisfies $CDF(\lambda_s, f'_{\text{agn}}) = 0.15865(0.02275)$. Any $f_{\text{agn}} < f'_{\text{agn}}$ should lie outside the $1\sigma(2\sigma)$ confidence interval (CI) of the probability distribution of f_{agn} . (ii) We keep increasing f_{agn} until we find $CDF(\lambda_s, f''_{\text{agn}}) = 0.5$. This f''_{agn} represents the median value of f_{agn} . (iii) We further increase f_{agn} until $CDF(\lambda_s, f'''_{\text{agn}}) > 1 - 0.15865(0.02275)$. Such f'''_{agn} determines the $1\sigma(2\sigma)$ upper bound of f_{agn} .

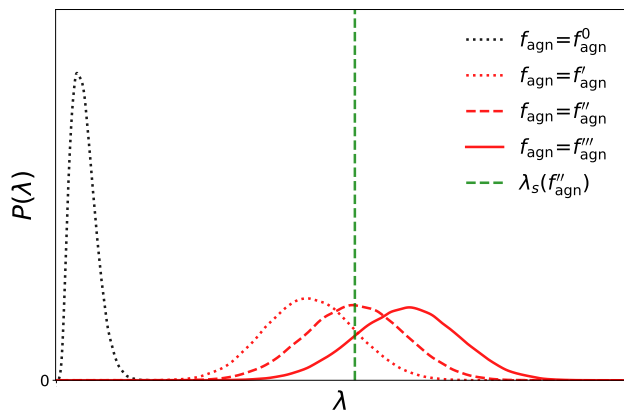


Figure 1. An example comparing the signal likelihood ratio $\lambda_s(f_{\text{agn}})$ (vertical green dashed line) with the conditional PDFs of λ for four different values of f_{agn} . In this example, $f_{\text{agn}}^0 = 0.1$, $f'_{\text{agn}} = 0.55$, $f''_{\text{agn}} = 0.7$, and $f'''_{\text{agn}} = 0.85$.

3. MOCK DATA

3.1. Population models of EMRIs

The EMRI rate is a primary feature of the EMRI population, and it is mainly determined by four factors (Babak et al. 2017): (i) the properties of the MBH population, including the mass function and spin distribution of MBHs; (ii) the $M - \sigma$ relation; (iii) the fraction of plunges among EMRIs; (iv) the characteristic masses of inspiralling stellar-mass compact objects. All of these factors are uncertain in astrophysics, and different conditions produce different EMRI population models. In this work, we adopt 11 EMRI population models proposed in Babak et al. (2017), i.e., from M1 to M12 (except the M11 model, which predicts a very low EMRI rate so that LISA and TianQin detecting almost no EMRIs, e.g., Babak et al. 2017; Fan et al. 2020). We set the eccentricities of EMRIs at plunge to be uniformly distributed in the range from 0 to 0.2. The main differences between the various models are summarized in Table I of Babak et al. (2017). When simulating the EMRIs originating in AGNs, we adjust the corresponding source parameters based on the population models presented in Pan et al. (2021), for instance, by updating the redshift distribution of EMRIs and setting all eccentricities at plunge to zero.

3.2. Mock observations

To estimate the abilities of detectors in constraining the cosmic expansion history and the formation channel of EMRIs, we need to simulate (i) the detected EMRI catalog, (ii) the redshift probability distribution of the candidate host galaxies, and (iii) the number of candidate host AGNs corresponding to each detected EMRI.

To generate a catalog of detected EMRIs, we follow the approach of Babak et al. (2017) and Fan et al. (2020). First, we adopt a galaxy catalog from the MultiDark cosmological simulations (Klypin et al. 2016; Croton et al. 2016) to select the host galaxies of the EMRIs. In the selection process, the mass of the MBH at the center of the selected host galaxy matches the mass of the MBH of the corresponding EMRI. Second, we generate the GW signals of EMRIs using the analytic kludge Kerr (AKK) waveform model (Barack & Cutler 2004; Babak et al. 2017). The reason for us to adopt this model is to facilitate comparison with the previous works (MacLeod & Hogan 2008; Laghi et al. 2021), although several new waveform models (Chua et al. 2017, 2021; Hughes et al. 2021; Isoyama et al. 2022) have been proposed recently. Third, we calculate the detector responses to the EMRI GW signals.

We consider three detector configurations, namely

- *TianQin* (TQ): the default situation in which three satellites form a constellation and operate

in a “3 months on + 3 months off” mode, with a mission lifetime of five years (Luo et al. 2016);

- *TianQin I+II* (TQ I+II): twin constellations of satellites with perpendicular orbital planes, that operate in a relay mode and can avoid the 3 months gap in data (Fan et al. 2020; Liang et al. 2022);
- *TianQin+LISA* (TQ+LISA): a network composed of TianQin and LISA, with the LISA configuration according to Amaro-Seoane et al. (2017). In this work, we assume that LISA and TianQin have a five year mission overlap and only consider EMRIs that are individually detectable by both TianQin and LISA. Here we emphasize that because both LISA (Colpi et al. 2024) and TianQin (Mei et al. 2021) are planned to be launched around 2035, it is possible that there will be a window of five years of overlap.

Finally, we set the threshold of SNR for GW detection to 20, and estimate the spatial localization errors of EMRIs with the Fisher information matrix (Cutler & Flanagan 1994; Vallisneri 2008).

For example, when using the M1 model (one can compare our results with those in Laghi et al. 2021), the distribution of the spatial localization errors (including the D_L estimation and sky localization errors) of various detector configurations are shown in Panels (a) and (b) of Figure 2. We find that the medians of the estimation errors for luminosity distance are about 7%, 6%, and 3% for TianQin, TianQin I+II, and TianQin+LISA, respectively, after accounting for additional systematic errors due to the weak lensing effects (Hirata et al. 2010; Cusin & Tamanini 2021) and peculiar velocities of the host galaxies (Kocsis et al. 2006). The corresponding median errors for sky localization are about 2.6 deg^2 , 0.8 deg^2 , and 0.02 deg^2 , respectively.

For the cosmological inferences, in order to simulate the redshift probability distributions of the detected EMRIs, we select their candidate host galaxies from the MultiDark galaxy catalog, and we take into account the selection effects of surveys. Here we set the limiting magnitude of the MultiDark galaxy catalog to $m_{\text{limit}}^* = +26 \text{ mag}$ according to the survey depth of the Chinese Space Station Telescope (CSST; Gong et al. 2019). To select the candidate host galaxies, we adopt a 2σ CI of the spatial localization error volumes, and convert the range of luminosity distance, $[D_{L;\text{min}}, D_{L;\text{max}}]$, into a range of redshift, $[z_{\text{min}}, z_{\text{max}}]$, using the relation-

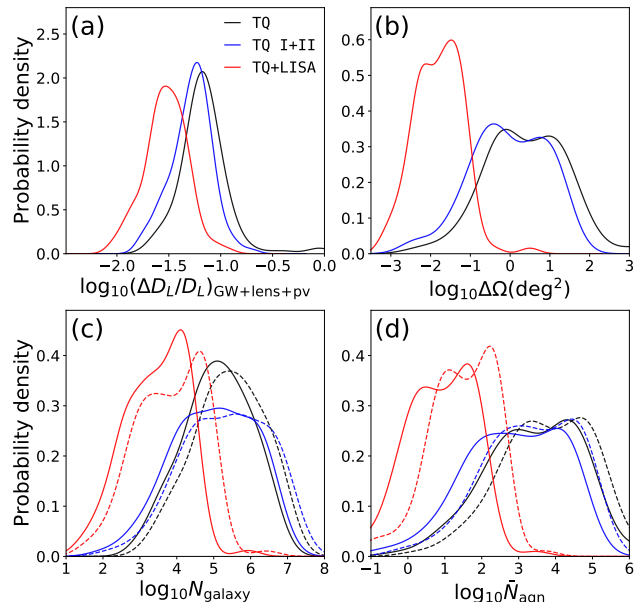


Figure 2. Panels (a), (b), (c), and (d) show, respectively, the distributions of the total D_L estimation errors, the sky localization errors, the numbers of the candidate host galaxies, and the expected numbers of the candidate host AGNs. All results are derived based on the M1 population model. The colors indicate TianQin (black), TianQin I+II (blue), and TianQin+LISA (red). And in Panels (c) and (d), the solid and dashed lines, respectively, represent the conditions in which the cosmological parameters are fixed and freely varying within a prior range, when transforming the range of luminosity distance into the range of redshift.

ship

$$D_{L;\text{min}} = c(1 + z_{\text{min}}) \int_0^{z_{\text{min}}} \frac{1}{H^-(z')} dz', \quad (20a)$$

$$D_{L;\text{max}} = c(1 + z_{\text{max}}) \int_0^{z_{\text{max}}} \frac{1}{H^+(z')} dz', \quad (20b)$$

where $H^-(z)$ and $H^+(z)$ are the minimum and maximum values of $H(z)$, respectively, given by the cosmological prior. For the prior, when we focus on the constraint on H_0 , we choose uniform distributions of $h \in \mathcal{U}[0.6, 0.8]$ and $\Omega_M \in \mathcal{U}[0.04, 0.5]$ while fixing $w_0 = -1$ and $w_a = 0$; when we are interested in the constraint on the dark energy EoS, we choose uniform distributions of $w_0 \in \mathcal{U}[-2, -0.5]$ and $w_a \in \mathcal{U}[-1, 1]$ while fixing h and Ω_M at their default values.

The distribution of the number of the candidate host galaxies is shown in Panel (c) of Figure 2. We can see that the typical number of candidate host galaxies for an EMRI detected by TianQin or TianQin I+II is about $10^5 - 10^6$ after accounting for the uncertainties in the cosmological parameters, and that the TianQin+LISA network can reduce the typical number to about $10^3 - 10^4$. In addition, to make the mock galaxy catalog more

realistic, we assume that all galaxies with $z > 0.6$ in the MultiDark galaxy catalog have photometric redshift (photo- z) errors which vary with the true redshifts z_{true} of the galaxies as

$$\sigma_{\text{photo-}z}(z_{\text{true}}) = \begin{cases} 0, & z_{\text{true}} \leq 0.6, \\ 0.03(1 + z_{\text{true}}), & z_{\text{true}} > 0.6, \end{cases} \quad (21)$$

(Dahlen et al. 2013; Zhou et al. 2021, 2022). The reason for setting the photo- z errors to zero for galaxies with $z \leq 0.6$ is that spectroscopic surveys of ground-based telescopes can cover this redshift range (Cui et al. 2012; Dawson et al. 2013; Aghamousa et al. 2016).

To constrain the formation channel of EMRIs, we estimate the expected number of AGNs λ_i within the spatial localization error volume ΔV_i of the i th EMRI according to the empirical bolometric AGN luminosity functions $\Phi(M^*, z)$ (Hopkins et al. 2007), where M^* represents the absolute magnitude of AGN, and then use this expectation to generate a Poisson distribution of random numbers. More quantitatively, we calculate the expectation λ_i with

$$\lambda_i = \Delta V_i \int_{-\infty}^{M_{\text{limit},i}^*} \Phi(M^*, z) dM^*, \quad (22)$$

where

$$M_{\text{limit},i}^* \approx m_{\text{limit}}^{\text{agn}} - 25 - 5 \lg \left(\frac{D_{L,i}}{1 \text{ Mpc}} \right) - BC$$

represents the observational limiting absolute magnitude for the candidate host AGN of the i th EMRI at a distance of $D_{L,i}$, and BC is a factor for bolometric correction (Duras et al. 2020). In this work, we set the limiting magnitude of the AGN survey to $m_{\text{limit}}^{\text{agn}} = +24.4$ mag according to the depth in the shallowest band of the CSST survey as well as taking into account the need for the spectroscopic identifications of AGNs (Gong et al. 2019). Taking the M1 model as an example, the distributions of the numbers of candidate host AGNs of the EMRIs for various detector configurations are shown in Panel (d) of Figure 2. We can see that for the same EMRI, the number of candidate host AGNs is about 1% of the number of the normal galaxies which are candidate hosts. This fraction is consistent with the AGN fraction among all galaxies.

4. CONSTRAINTS ON COSMOLOGICAL PARAMETERS

In this section, we use the Bayesian framework described in Section 2.2 to calculate the posterior probability distributions of various cosmological parameters, including the standard Λ CDM model parameters

(H_0, Ω_M) and the dark energy EoS parameters (w_0, w_a). The essence of the computational process is fitting the $D_L - z$ relation with Markov Chain Monte-Carlo (MCMC) sampling. In the following, we adopt a total of 11 population models, from M1 to M12 except M11, to evaluate the capability of future EMRI observations in constraining the cosmological parameters.

4.1. Constraints on H_0 and Ω_M

We first fit the $D_L - z$ relation, using the luminosity distances from EMRI observations and the redshifts extracted from galaxy surveys. The result is shown in Figure 3, and the corresponding constraints on H_0 and Ω_M are shown in Figure 4. Note that in this section we fix the parameters of the dark energy EoS to $w_0 = -1$ and $w_a = 0$.

For the Hubble-Lemaître constant H_0 , under the fiducial population model, i.e., the M1 model, the expected error is about 8.1% for TianQin, and TianQin I+II can reduce this error to about 4.4%. Under the other population models from M2 to M12, the error of H_0 varies considerably from model to model. The variations are mainly caused by the fact that the detection rates of EMRIs predicted by various models vary considerably (see Babak et al. 2017; Fan et al. 2020). In general, TianQin is able to achieve a precision in the range of about 3.4% – 9.6%, while that for TianQin I+II is expected to be in the range of about 1.5% – 7.2%.

For the fractional matter density parameter Ω_M , in almost all population models the TianQin configuration cannot provide reasonable constraint (comparing the error scales corresponding to the priors and the posteriors), except for the M6, M7, and M12 models. But TianQin I+II can significantly improve the constraint on Ω_M . More quantitatively, under the M6, M7, and M12 models, TianQin is likely to constrain Ω_M to a precision of about 46%, 33%, and 42%, respectively, whereas TianQin I+II would be able to constrain Ω_M to a precision of about 29%, 13%, and 11%, respectively.

If TianQin and LISA could form a network, i.e., TianQin+LISA, the constraints on H_0 and Ω_M are significantly improved in all population models, as is shown by the red error bars in Figure 4. For example, in the M1 model, the errors of H_0 and Ω_M can shrink to about 1.9% and 20%, respectively. Under the other models, the precision of H_0 can be improved to about 0.4% – 7.1%, and the error of Ω_M would reduce to the range of about 13% – 43%. For completeness, we summarize the expected precisions on H_0 and Ω_M for various cases in Table I.

In addition, the importance of improving the sky localization by employing the TianQin+LISA network can

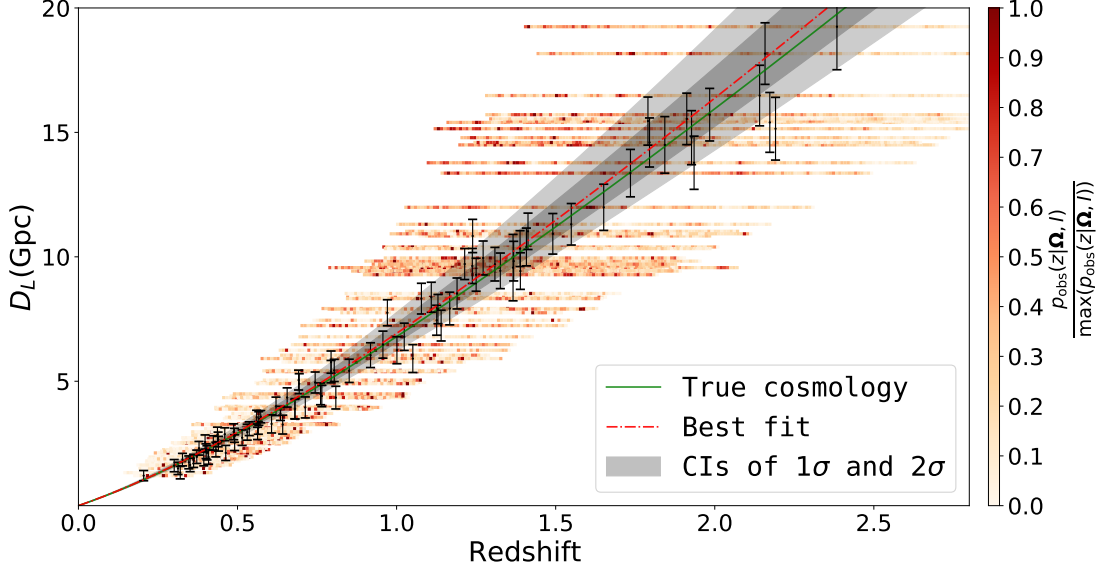


Figure 3. Typical example of fitting the $D_L - z$ relation which is derived from the EMRI dark sirens detectable by the TianQin+LISA network. Here we use the fiducial EMRI population model. The horizontal colored serial squares represent the probability distribution of redshift (normalized by the maximum) derived from the observed candidate host galaxies, and the color hues from white to red show the probability of redshift. The luminosity distances shown here represent the mean values, and their errors (1σ CI) are indicated by the black error bars. The solid green line represents the true cosmological model adopted by our simulations. The dot-dashed red line represents the best-fit cosmological model, while the two shaded regions represent the 1σ and 2σ CIs.

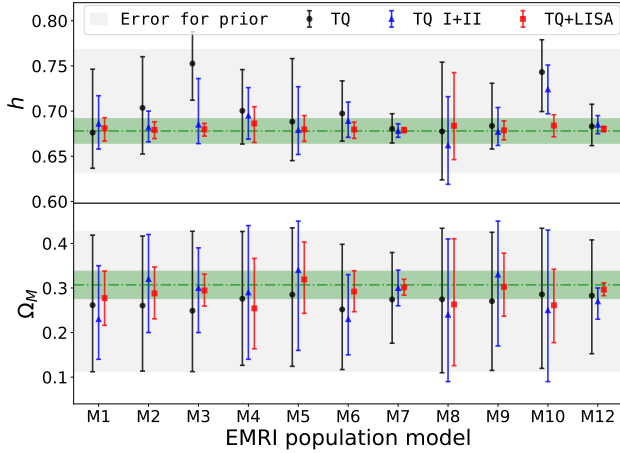


Figure 4. Constraints on h and Ω_M given by the EMRIs detectable by TianQin (black), TianQin I+II (blue), and TianQin+LISA (red). The horizontal axis represents the different EMRI population models. The error bars correspond to an 1σ CI. The gray-shaded area represents the 1σ equivalent error of the prior, and the green-shaded region represents an error scale of 2% (10%) for h (Ω_M).

be clearly seen in the upper panel of Figure 4. In particular, under Models M3 and M10, the posterior of h provided by a single detector, such as TianQin or TianQin I+II, could be significantly biased with respect to the true value. The bias is related to the paucity of EMRIs that can be precisely localized [see Panel (b) of

Figure 2], which increases the fluctuation in the posterior distribution of the redshift of an EMRI. Using TianQin+LISA, however, more EMRIs can be precisely localized, and the precision reduces the fluctuation of the redshift distribution function for each EMRI. We notice that a similar trend can be seen in earlier studies (Laghi et al. 2021; Muttoni et al. 2022; Zhu et al. 2022a,b).

4.2. Constraints on w_0 and w_a

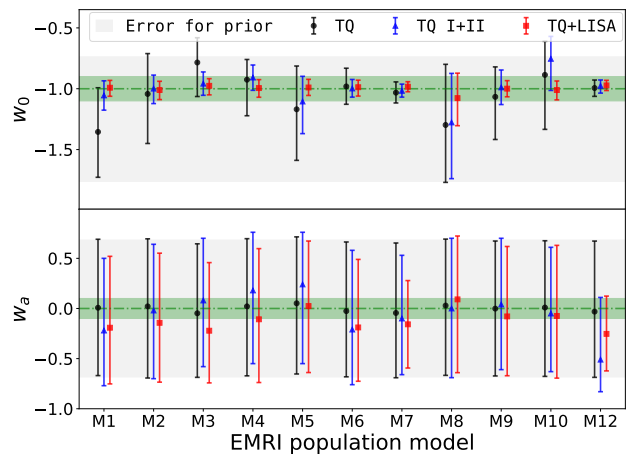


Figure 5. Same as Figure 4, but for w_0 and w_a . The green shades represent error scales of $\Delta w_0 = 0.1$ and $\Delta w_a = 0.1$.

The errors on the dark energy EoS parameters w_0 and w_a are shown in Figure 5. Here we fix $h = 0.678$ and $\Omega_M = 0.307$. We find that only w_0 can be effectively constrained and w_a is not constrained in almost all population models. Even under the M7 and M12 models, despite the fact that they have optimistic EMRI rates such that TianQin I+II and TianQin+LISA can detect a total number of more than one thousand EMRIs, still, a stringent constraint on w_a cannot be obtained. The much better constraint on w_0 than on w_a implies that reconstructing the evolution of the dark energy with redshift requires much better EMRIs than those needed to infer the deviation of the dark-energy EoS with respect to the value $w = -1$ of the standard model.

More specifically, under the fiducial population model, the error of w_0 can reach about 37% for TianQin, about 12% for TianQin I+II, and about 6.5% for TianQin+LISA. Under the other population models, i.e., from M2 to M12 except M11, the expected errors of w_0 can reach 6.7% – 48% for TianQin, about 5.4% – 43% for TianQin I+II, and about 4.2% – 22% for TianQin+LISA. Similar to the constraints on H_0 , the errors on w_0 also vary considerably across population models. Finally, in Table I we also summarize the expected precisions in the constraints on w_0 and w_a for various models.

5. CONSTRAINING THE FORMATION CHANNEL OF EMRIS

So far, we have assumed that each candidate host galaxy has the same probability of hosting an EMRI, be it a normal galaxy or an AGN. Now we drop this assumption and use the statistical framework described in Section 2.3 to constrain f_{agn} , which is the fraction of EMRIs which reside in AGNs. Since the statistical significance increases with the number of GW sources, we denote $N_{\text{GW},3\sigma}^{\text{threshold}}$ as the minimum number of detected EMRIs that is required to reject the null hypothesis at a significance level of 3σ , and we study its dependence on the value of f_{agn} .

Here, we follow the works of Babak et al. (2017) and Pan et al. (2021) to generate the MBH mass function and its evolution with redshift. Correspondingly, the dimensionless MBH spin is set to 0.98 and the mass of the stellar BH is fixed at $10 M_\odot$. The above choices are commonly used in the previous works (Barausse 2012; Amaro-Seoane et al. 2013; Abbott et al. 2019b, 2023b), thus we adopt them for easier comparison with the previous works. The eccentricities of EMRIs are expected to be significantly different in different models. For the EMRIs in normal galaxies, we assumed a uniform distribution of the eccentricities at plunge within the range

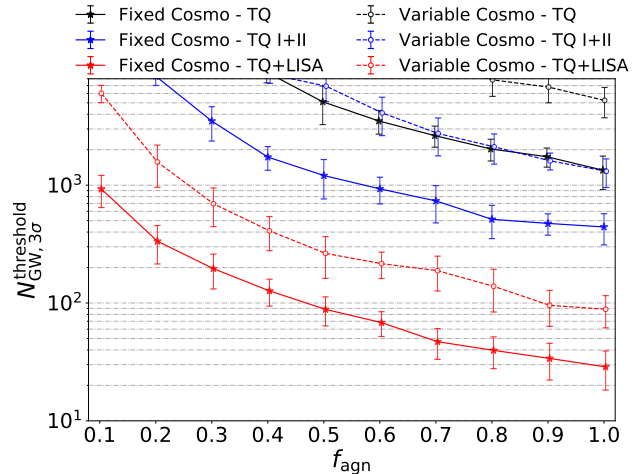


Figure 6. Minimum number $N_{\text{GW},3\sigma}^{\text{threshold}}$ of detected EMRI events required to testify the EMRI-AGN correlation with a 3σ significance. The black, blue, and red error bars and lines correspond to TianQin, TianQin I+II, and TianQin+LISA observations. The solid lines represent the case in which both H_0 and Ω_M are fix to the true values, and the dashed lines with corresponding error bars represent the case in which both H_0 and Ω_M are freely variable within the prior. The error bars correspond to 1σ CI.

of $[0, 0.2]$, as is proposed by Babak et al. (2017); for the EMRIs originating in AGNs, we set their eccentricities to zero, to account for the damping of eccentricity suggested by Pan et al. (2021). When we convert the error of luminosity distance to the redshift error using Equations (20a) and (20b), we assume two cosmological conditions, namely: (i) “fixed cosmology” in which the cosmological parameters are fixed to their true values, and (ii) “variable cosmology” where the cosmological parameters H_0 and Ω_M are freely variable within their priors. We consider the latter condition to account for the tension in the current measurements of the Hubble constant (Freedman 2017; Aghanim et al. 2020; Riess et al. 2021; Di Valentino et al. 2021; Perivolaropoulos & Skara 2022). The resulting dependence of the required minimum number $N_{\text{GW},3\sigma}^{\text{threshold}}$ on the fraction f_{agn} is shown in Figure 6. We can see that $N_{\text{GW},3\sigma}^{\text{threshold}}$ decreases with increasing f_{agn} in all cases.

In the “fixed cosmology” condition, TianQin would need to detect at least 1300 EMRIs to be able to reject the null hypothesis and establish the EMRI-AGN correlation if $f_{\text{agn}} = 1$. Under the same condition, TianQin I+II needs to detect at least about 450 EMRIs and TianQin+LISA needs to detect at least about 30 EMRIs. In the “variable cosmology” condition, if $f_{\text{agn}} = 1$ the minimum number $N_{\text{GW},3\sigma}^{\text{threshold}}$ required for TianQin, TianQin I+II, and TianQin+LISA are about 5000, 1300, and 90, respectively. The increase of $N_{\text{GW},3\sigma}^{\text{threshold}}$ in the

Table I. Expected relative errors of the Λ CDM cosmological model parameters (H_0, Ω_M) and the CPL dark energy model parameters (w_0, w_a) for the 11 EMRI population models and assuming three different detector configurations: TianQin, TianQin I+II and TianQin+LISA. The bar “—” means no effective constraint.

EMRI population model	Expected relative error											
	TianQin				TianQin I+II				TianQin+LISA			
	$\frac{\Delta H_0}{H_0}$	$\frac{\Delta \Omega_M}{\Omega_M}$	$ \frac{\Delta w_0}{w_0} $	$\frac{\Delta w_a}{1}$	$\frac{\Delta H_0}{H_0}$	$\frac{\Delta \Omega_M}{\Omega_M}$	$ \frac{\Delta w_0}{w_0} $	$\frac{\Delta w_a}{1}$	$\frac{\Delta H_0}{H_0}$	$\frac{\Delta \Omega_M}{\Omega_M}$	$ \frac{\Delta w_0}{w_0} $	$\frac{\Delta w_a}{1}$
M1	8.1%	—	37%	—	4.4%	34%	12%	—	1.9%	20%	6.5%	—
M2	7.9%	—	37%	—	2.5%	36%	12%	—	1.4%	19%	7.5%	—
M3	5.6%	—	24%	—	5.3%	31%	9.6%	—	1.0%	12%	6.7%	—
M4	6.1%	—	23%	—	4.2%	—	10%	—	2.9%	33%	7.2%	—
M5	8.3%	—	39%	—	5.5%	47%	24%	—	2.1%	26%	6.6%	—
M6	4.9%	46%	15%	—	2.9%	29%	7.3%	—	1.3%	15%	6.5%	—
M7	2.4%	33%	8.7%	—	1.1%	13%	5.4%	—	0.4%	5.8%	4.1%	44%
M8	9.6%	—	48%	—	7.2%	—	43%	—	7.1%	46%	22%	—
M9	5.4%	—	30%	—	3.1%	46%	14%	—	1.6%	23%	6.6%	—
M10	5.9%	—	36%	—	4.0%	—	22%	—	1.8%	27%	7.8%	—
M12	3.4%	42%	6.7%	—	1.5%	11%	5.4%	47%	0.4%	4.7%	4.2%	37%

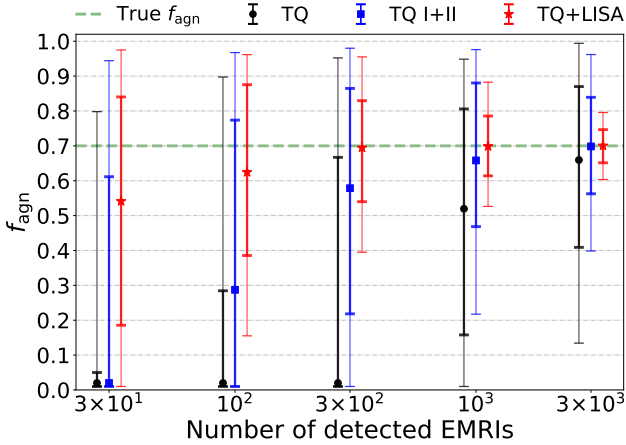


Figure 7. The error in constraining f_{agn} as a function of the number of detected EMRIs. Here we fix the cosmological parameters to their true values. The black, blue, and red error bars correspond to TianQin, TianQin I+II, and TianQin+LISA. The thick and thin error bars correspond to 1σ and 2σ CIs, respectively. The dots in the middle of the error bars represent the expectations. The green dashed horizontal line represents the injected f_{agn} in the simulations.

case of variable cosmology is caused by an increase of the redshift range when transforming the luminosity distance range into the redshift space. For different cases, $N_{\text{GW},3\sigma}^{\text{threshold}}$ as a function of f_{agn} can be approximate as $N_{\text{GW},3\sigma}^{\text{threshold}} \propto f_{\text{agn}}^{-1.6}$.

After testing the EMRI-AGN correlation, we proceed to estimate the value of f_{agn} using Equation (19) and Monte-Carlo simulations. As an illustration, we set the fraction of EMRIs originating in AGNs to $f_{\text{agn}} = 0.7$.

The variation of the error of f_{agn} with the number of detected EMRIs for different detector configurations is shown in Figure 7. We find that as the number of detected EMRIs approaches or exceeds the threshold number $N_{\text{GW},3\sigma}^{\text{threshold}}$ (refer to Figure 6), the constraint on f_{agn} converges toward the injected value, with the constraining error diminishing as the number of detected EMRIs increases. When the number of detected EMRIs is considerably lower than $N_{\text{GW},3\sigma}^{\text{threshold}}$, the constraint on f_{agn} is consistent with $f_{\text{agn}} = 0.01$ (the fraction of AGNs among all galaxies we assumed), but with large error. Furthermore, for an equivalent number of EMRI detections, the TianQin+LISA network significantly enhances the precision of constraining f_{agn} . For instance, with 1000 EMRI detections, the errors corresponding to 1σ CIs are $\Delta f_{\text{agn}} \sim 0.33$ for TianQin and $\Delta f_{\text{agn}} \sim 0.21$ for TianQin I+II, whereas the error for TianQin+LISA shrinks to $\Delta f_{\text{agn}} \sim 0.09$.

We would like to note that the real EMRI population in the universe is more completed than the modeled ones presented in this work. For examples, both the spins of the MBHs (Sesana et al. 2014; Bustamante & Springel 2019; Sisk-Reynés et al. 2022) and the masses of the stellar-mass BHs (Pan et al. 2022; Abbott et al. 2023b) should follow certain distributions, but we have adopted fixed values for them. In addition, the EMRIs originating in normal galaxies (Hopman et al. 2007; Yunes et al. 2008; Berry & Gair 2013; Amaro-Seoane 2019; Han et al. 2020; Fan et al. 2022) or in those post-merger galaxies hosting MBHBs (Mazzolari et al. 2022; Naoz et al. 2022; Naoz & Haiman 2023) may exhibit eccentricities much higher than 0.2, and in AGNs the stellar-mass BHs

would interact with the accretion disks (Yunes et al. 2011; Chatterjee et al. 2023). All these factors could affect the duration, GW amplitude, or extra modes of an EMRI, and consequently affect its detectability. Nevertheless, our work serves as a key step towards testing the EMRI-AGN correlation.

6. DISCUSSIONS

6.1. Advantage of combining EMRIs with AGN observation

Once either of the following two conditions is met, we can use AGN catalogs to extract the redshift information of a detected EMRI (or at least assign higher weights to the AGNs): (i) the fraction of the EMRIs originate in AGNs, f_{agn} , is statistically constrained to be close to 1 by our method; and (ii) the detected EMRI has a zero eccentricity at the time of plunge (see, e.g., Pan & Yang 2021; Pan et al. 2021; Amaro-Seoane et al. 2023, for explanation). We note that LISA and TianQin can measure the eccentricities of EMRIs to a precision of $\Delta e \approx 10^{-6}$ (Babak et al. 2017; Fan et al. 2020), so they can differentiate the formation channels.

Assuming that all EMRIs come from AGNs, and using only the AGN catalog to look for the candidate hosts for EMRIs, we repeat the simulation shown in Section 3.2 and derive the posteriors for the cosmological parameters. More specifically, we consider the EMRIs detected by TianQin in the M1 population model as an example. The AGN catalog is based on the MultiDark catalog but we use the limiting magnitude of CSST to select observable AGNs. The result is shown in Figure 8. We find that the constraints on cosmological parameters are improved. More quantitatively, by switching from the galaxy catalog to the AGN catalog, the precision of H_0 improves from about 3.7% to about 3.2%, and the precision of w_0 improves from about 25% to about 13%. For a fair comparison, here we do not consider the redshift errors in either candidate host galaxies or AGNs.

These improvements mainly benefit from the fact that AGNs constitute only about (1 – 10)% of all galaxies (e.g., compare the galaxy and AGN luminosity functions in Dahlen et al. 2005; Hopkins et al. 2007). When f_{agn} is close to 1 or the detected EMRIs have zero eccentricities at plunge, we can derive more precisely the redshifts of EMRIs with the help of AGN catalogs. These results also imply that circular EMRIs are better than those eccentric ones in constraining cosmological parameters.

In addition, we would like to point out that EMRIs may be accompanied by EM counterparts (Wang et al. 2019b, 2022b; Li et al. 2023; Amaro-Seoane et al. 2023). The EM signals could be detected by the current and planned time-domain survey telescopes, such as

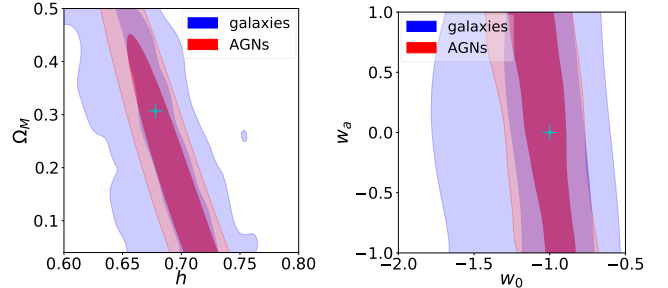


Figure 8. Constraints on (h, Ω_M) (left panel) and (w_0, w_a) (right panel) by combining the EMRIs detected by TianQin with AGN catalogs. The eccentricities at plunges are set to zero, and the other parameters are derived from the M1 model. The blue contours represent the constraints derived from candidate host galaxies and the red contours represent the constraints from candidate host AGNs. The two levels of contours correspond to 1σ and 2σ CIs, respectively. The cyan crosses mark the injected cosmological parameters in our simulations.

the Wide Field Survey Telescope (WFST) (Wang et al. 2023; Huang et al. 2024), the Multi-channel Photometric Survey Telescope (Mephisto) (Yuan et al. 2020), Vera Rubin Observatory (also known as LSST; Ivezić et al. 2019), the Einstein Probe (Yuan et al. 2015), Athena (Nandra et al. 2013; McGee et al. 2020), the Five-Hundred Aperture Spherical Radio Telescope (FAST) (Nan et al. 2011), or the Square Kilometre Array (SKA) (Janssen et al. 2015). Detecting an EM counterpart could help us narrow down the candidates host galaxies, or even uniquely identify the host galaxy of an EMRI. Such detections will enable us to not only improve the precisions of the cosmological parameters due to the more accurate redshift information of the EMRIs, but also better understand the formation channel of EMRIs.

6.2. Effects of eccentricity on the spatial localization of EMRIs

In our simulations, we have set the eccentricities of EMRIs (at plunge) to be uniformly distributed in the range of 0 to 0.2 when simulating the EMRIs from normal galaxies, and set them to zero when the EMRIs come from AGNs (Pan & Yang 2021; Pan et al. 2022, 2021; Amaro-Seoane et al. 2023). To evaluate whether the eccentricities of EMRIs may affect the precision in the measurement of their parameters, here we analyze the spatial localization errors for the EMRIs formed in different channels. The results are shown in Figure 9.

From Figure 9, we can see that the effect of eccentricity at plunge is weak on the spatial localization errors (sky position and distance). The weak dependence implies that neither the errors on the cosmological parameters presented in Section 4 nor the required mini-

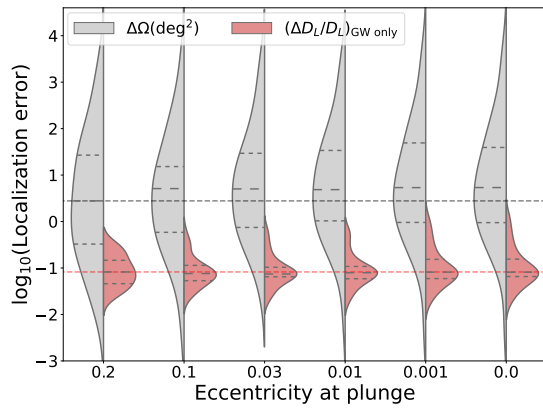


Figure 9. Spatial localization errors of the TianQin EMRIs as a function of their eccentricities at the time of plunge. The gray (red) violinplots represent the probability distributions for the sky localizations errors (D_L estimation errors) of EMRIs, and the gray (red) horizontal dashed line shows the median of the corresponding error.

imum number of EMRIs for establishing the EMRI-AGN correlation presented in Section 5 is sensitive to our assumption of the distribution of EMRI eccentricities.

Although we have not considered in detail in this work, a special case worth mentioning is an EMRI whose eccentricity is close to unity. Such a system may occasionally form in a normal galaxy, and it would radiate multiple GW bursts before transitioning into the inspiraling phase (Rubbo et al. 2006; Hopman et al. 2007; Yunes et al. 2008; Berry & Gair 2013; Amaro-Seoane 2019; Han et al. 2020; Fan et al. 2022). The SNR of this extreme-mass-ratio burst (EMRB) may exceed the detection threshold, allowing identification of individual bursts (Rubbo et al. 2006; Yunes et al. 2008; Han et al. 2020; Fan et al. 2022; Wu et al. 2023). Detecting these burst prior to an EMRI signal can enhance the spatial localization of the EMRI by partially breaking the degeneracy between parameters (Barack & Cutler 2004; Mikóczy et al. 2012; Xuan et al. 2023). This prospect deserves future investigation.

6.3. Prospect of clarifying the Hubble tension

Recently, the cosmological standard model—flat- Λ CDM, is challenged by the Hubble tension (Freedman 2017; Di Valentino et al. 2021; Perivolaropoulos & Skara 2022). The H_0 obtained from the flat- Λ CDM model plus cosmic microwave background is $67.4 \pm 0.5 \text{ km s}^{-1} \text{ Mpc}^{-1}$, with a relative error of about 0.7% (Aghanim et al. 2020), and the H_0 from the cosmic distance ladders and type Ia supernovae is $73.2 \pm 1.3 \text{ km s}^{-1} \text{ Mpc}^{-1}$, with a relative error of about 1.8% (Riess et al. 2021). So if we want to clarify the Hubble tension by a new independent

measurement, the independently measured H_0 needs to be better than a precision of about 2%.

We can see from Table I that TianQin does not achieve a precision of 2% in constraining H_0 under the EMRI population models considered in this paper. As for TianQin I+II, it achieves a precision better than 2% only under the population models with optimistic EMRI rates, such as the M7 and M12 models. However, the multi-detector network formed by LISA and TianQin, i.e., TianQin+LISA, can much better constrain H_0 . For example, under most of the population models, except for the M8 and M11 models, the TianQin+LISA network can constrain H_0 to a precision of near or better than 2%. Therefore, our results support a joint observation of GWs by TianQin and LISA.

7. CONCLUSION

In this work, we have investigated the potential of using EMRIs as dark sirens to constrain the cosmological parameters as well as infer the formation channel of EMRIs. We adopted 11 population models presented in Babak et al. (2017) to generate catalogs of EMRIs which are detectable by different space GW detectors or detector networks.

(i) To constrain the cosmological parameters, we derived the redshift probability distributions of detected EMRIs by matching their spatial localization error volumes with galaxy survey catalogs, and then evaluated the posterior probability distributions of the cosmological parameters via a Bayesian analytical framework. Our results show that precise constraints on the Hubble-Lemaître constant H_0 and the dark energy EoS parameter w_0 can be obtained from EMRIs. Under the fiducial population model M1, the precision of H_0 can reach about 8.1% for TianQin, about 4.4% for TianQin I+II, and about 1.9% for the TianQin+LISA network; and the precision of w_0 can reach about 37% for TianQin, about 12% for TianQin I+II, and about 6.5% for the TianQin+LISA network. Additionally, under the most optimistic EMRI population model, TianQin can constrain H_0 and w_0 to a precision better than about 3% and about 10%, and the TianQin+LISA network can constrain H_0 and w_0 to a precision better than about 1% and about 5%, respectively.

(ii) To constrain the formation channel of EMRIs, we adopted an AGN luminosity function to self-consistently generate the numbers of candidate host AGNs for the detected EMRIs, and then used the Poisson distribution to statistically test the spatial correlation between EMRIs and AGNs. We mainly found that the minimum number $N_{\text{GW},3\sigma}^{\text{threshold}}$ of the EMRIs required to establish the EMRI-AGN correlation decreases with increasing

f_{agn} . If $f_{\text{agn}} = 1$ and the cosmological parameters are fixed, the values of $N_{\text{GW},3\sigma}^{\text{threshold}}$ for the three detector configurations, namely TianQin, TianQin I+II, and TianQin+LISA, are about 1300, 450, and 30 respectively. Under the condition that the cosmological parameters vary freely within the priors, the values of $N_{\text{GW},3\sigma}^{\text{threshold}}$ become significantly larger, by a factor of about three or larger. However, in our simulated cases where the correlation between EMRIs and AGNs can be statistically confirmed, a combination of the EMRI and AGN catalogs can significantly improve the constraints on the cosmological parameters.

The cosmological constraints reported in this work appear to be somewhat weaker than those of LISA alone reported in Laghi et al. (2021) (also see MacLeod & Hogan 2008). For example, under the M1, M5, and M6 models, LISA with a four year mission is expected to constrain H_0 and w_0 to higher precisions than TianQin or TianQin I+II. This is mainly because the most sensitive band of TianQin is slightly higher than that of LISA, which makes the EMRI detection rate of TianQin much lower than LISA (Babak et al. 2017; Fan et al. 2020). However, we would like to point out that currently there is large uncertainty in the mass function of MBHs especially at the low mass end (Greene & Ho 2007; Barausse 2012; Gallo & Sesana 2019; He et al. 2024). The GW signals radiated by the EMRIs that are formed by lighter MBHs, will have higher frequencies and are more easily detected by TianQin.

Our results also demonstrate the prospect of using space-borne GW detectors to statistically infer the formation channel of EMRIs. It is previously known that the intrinsic parameters of an EMRI, such as the eccentricity at plunge (Pan & Yang 2021; Pan et al. 2021) and the spin of the MBH (Burke et al. 2020), can help us infer the formation channel of the EMRI, but an unbiased extraction of the intrinsic parameters relies heavily on an accurate EMRI waveform model (Chua et al. 2017; Amaro-Seoane 2018; Torres-Orjuela et al. 2021). Now the effectiveness of the statistical framework proposed in this work mainly relies on the spatial localization accu-

racies of EMRIs and the completeness of AGN catalogs. Since the localization accuracies are mainly determined by the SNRs of the EMRIs and the completeness of the AGN catalogs is mainly determined by the depths of AGN surveys, the demand of accurate waveform model subsides to a secondary role. In this sense, our statistical framework could serve as a useful complementary means of inferring the formation channel of EMRIs.

ACKNOWLEDGEMENTS

The authors would like to thank Linhua Jiang, Yuming Fu, Zhenwei Lyu, Zhen Pan and Tieguaung Zi for very helpful discussions, thank the anonymous referee for many helpful comments, and thank the Theoretical Astrophysical Observatory (TAO; <https://tao.asvo.org.au/tao/>) for providing access to the download of the mock galaxy catalogs. This work is supported by the National Key Research and Development Program of China (Grant No. 2021YFC2203002) and the National Natural Science Foundation of China (Grant No. 11991053). L.-G. Zhu is funded by China Postdoctoral Science Foundation (Grant No. 2023M740113), H.-M. Fan is supported by the Hebei Natural Science Foundation (Grant No. A2023201041), Y.-M. Hu is supported by the Natural Science Foundation of China (Grants No. 12173104 and No. 12261131504), and Guangdong Major Project of Basic and Applied Basic Research (Grant No. 2019B030302001), and J.-d. Zhang is supported by the Guangdong Basic and Applied Basic Research Foundation (Grant No. 2023A1515030116). This work is also supported by Key Laboratory of TianQin Project (Sun Yat-sen University), Ministry of Education. The computations in this work was performed on the High Performance Computing Platform of the Centre for Life Science, Peking University.

Software: numpy (van der Walt et al. 2011), scipy (Virtanen et al. 2020), emcee (Foreman-Mackey et al. 2013, 2019), matplotlib (Hunter 2007), corner (Foreman-Mackey 2016), GetDist (Lewis 2019), and seaborn (Waskom 2021).

APPENDIX

A. DISTRIBUTIONS OF THE LIKELIHOOD RATIO IN THE NULL AND ALTERNATIVE HYPOTHESES

In this appendix we illustrate a deviation of the distribution of the likelihood ratio from the background distribution as f_{agn} , the fraction of EMRIs originated in AGNs, increases. We assume that 100 EMRIs are detected by the TianQin+LISA network, which is expected by most population models for five years of observation, regardless of whether EMRIs originate predominantly in normal galaxies or AGNs (Babak et al. 2017; Fan et al. 2020; Pan et al. 2021). The background distributions $P_{\text{bg}}(\lambda)$ of the likelihood ratio are shown in Figure 10 as the dashed lines, while the probability distributions $P(\lambda)$ of the “signal” likelihood ratio (derived from detected EMRIs) are represented by solid

lines (we wish to clarify that the signal likelihood ratio λ is a deterministic function of f_{agn} in actual GW detections). Both distributions $P_{\text{bg}}(\lambda)$ and $P(\lambda)$ are derived from tens of thousands of independently repeated simulations. We can see that the variation of $P(\lambda)$ is more significant than $P_{\text{bg}}(\lambda)$ as f_{agn} increases. This discrepancy arises because the variation of $P(\lambda)$ is caused by a combination of the increase in the parameter f_{agn} and the resulting increasing number of candidate host AGNs $\{N_{\text{agn},i}\}$, whereas the variation of $P_{\text{bg}}(\lambda)$ solely stems from the change in the parameter f_{agn} .

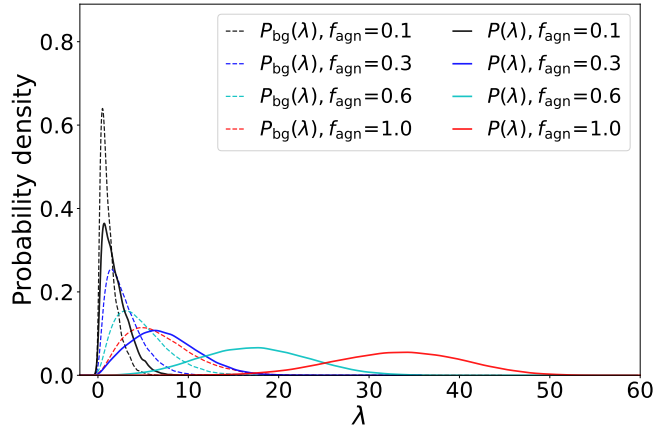


Figure 10. Typical background distribution $P_{\text{bg}}(\lambda)$ (dashed line) and probability distribution $P(\lambda)$ (solid line) of the likelihood ratio λ in Equation (18) for 100 EMRIs detected by TianQin+LISA, assuming our fiducial cosmological parameters. The black, blue, cyan, and red colors correspond to four fractions of $f_{\text{agn}} = 0.1, 0.3, 0.6, 1.0$, respectively.

REFERENCES

- Abbott, B. P., Abbott, R., Abbott, T. D., et al. 2016, Phys. Rev. Lett., 116, 061102, doi: [10.1103/PhysRevLett.116.061102](https://doi.org/10.1103/PhysRevLett.116.061102)
- . 2017a, Phys. Rev. Lett., 119, 161101, doi: [10.1103/PhysRevLett.119.161101](https://doi.org/10.1103/PhysRevLett.119.161101)
- . 2017b, Nature, 551, 85, doi: [10.1038/nature24471](https://doi.org/10.1038/nature24471)
- . 2017c, Astrophys. J. Lett., 848, L12, doi: [10.3847/2041-8213/aa91c9](https://doi.org/10.3847/2041-8213/aa91c9)
- . 2019a, Physical Review X, 9, 031040, doi: [10.1103/PhysRevX.9.031040](https://doi.org/10.1103/PhysRevX.9.031040)
- . 2019b, Astrophys. J. Lett., 882, L24, doi: [10.3847/2041-8213/ab3800](https://doi.org/10.3847/2041-8213/ab3800)
- . 2020a, Living Reviews in Relativity, 23, 3, doi: [10.1007/s41114-020-00026-9](https://doi.org/10.1007/s41114-020-00026-9)
- . 2021a, Astrophys. J., 909, 218, doi: [10.3847/1538-4357/abdc67](https://doi.org/10.3847/1538-4357/abdc67)
- Abbott, R., Abbott, T. D., Abraham, S., et al. 2020b, Astrophys. J. Lett., 900, L13, doi: [10.3847/2041-8213/aba493](https://doi.org/10.3847/2041-8213/aba493)
- . 2021b, Physical Review X, 11, 021053, doi: [10.1103/PhysRevX.11.021053](https://doi.org/10.1103/PhysRevX.11.021053)
- . 2021c, Phys. Rev. Lett., 126, 241102, doi: [10.1103/PhysRevLett.126.241102](https://doi.org/10.1103/PhysRevLett.126.241102)
- Abbott, R., Abbott, T. D., Acernese, F., et al. 2023a, Physical Review X, 13, 041039, doi: [10.1103/PhysRevX.13.041039](https://doi.org/10.1103/PhysRevX.13.041039)
- . 2023b, Physical Review X, 13, 011048, doi: [10.1103/PhysRevX.13.011048](https://doi.org/10.1103/PhysRevX.13.011048)
- Abbott, R., Abe, H., Acernese, F., et al. 2021d, arXiv e-prints, arXiv:2112.06861, doi: [10.48550/arXiv.2112.06861](https://doi.org/10.48550/arXiv.2112.06861)
- . 2023c, Astrophys. J., 949, 76, doi: [10.3847/1538-4357/ac74bb](https://doi.org/10.3847/1538-4357/ac74bb)
- Acernese, F., Agathos, M., Ain, A., et al. 2023, in Journal of Physics Conference Series, Vol. 2429, Journal of Physics Conference Series, 012040, doi: [10.1088/1742-6596/2429/1/012040](https://doi.org/10.1088/1742-6596/2429/1/012040)
- Agazie, G., Anumarlapudi, A., Archibald, A. M., et al. 2023, Astrophys. J. Lett., 951, L8, doi: [10.3847/2041-8213/acdac6](https://doi.org/10.3847/2041-8213/acdac6)
- Aghamousa, A., Aguilar, J., Ahlen, S., et al. 2016, arXiv e-prints, arXiv:1611.00036, doi: [10.48550/arXiv.1611.00036](https://doi.org/10.48550/arXiv.1611.00036)
- Aghanim, N., Akrami, Y., Ashdown, M., et al. 2020, Astron. Astrophys., 641, A6, doi: [10.1051/0004-6361/201833910](https://doi.org/10.1051/0004-6361/201833910)

- Amaro-Seoane, P. 2018, *Living Reviews in Relativity*, 21, 4, doi: [10.1007/s41114-018-0013-8](https://doi.org/10.1007/s41114-018-0013-8)
- . 2019, *Phys. Rev. D*, 99, 123025, doi: [10.1103/PhysRevD.99.123025](https://doi.org/10.1103/PhysRevD.99.123025)
- Amaro-Seoane, P., Andrews, J., Arca Sedda, M., et al. 2023, *Living Reviews in Relativity*, 26, 2, doi: [10.1007/s41114-022-00041-y](https://doi.org/10.1007/s41114-022-00041-y)
- Amaro-Seoane, P., Audley, H., Babak, S., et al. 2017, arXiv e-prints, arXiv:1702.00786, doi: [10.48550/arXiv.1702.00786](https://doi.org/10.48550/arXiv.1702.00786)
- Amaro-Seoane, P., Sopuerta, C. F., & Freitag, M. D. 2013, *Mon. Not. R. Astron. Soc.*, 429, 3155, doi: [10.1093/mnras/sts572](https://doi.org/10.1093/mnras/sts572)
- Antoniadis, J., Arumugam, P., Arumugam, S., et al. 2023, *Astron. Astrophys.*, 678, A50, doi: [10.1051/0004-6361/202346844](https://doi.org/10.1051/0004-6361/202346844)
- Arun, K. G., Mishra, C. K., Van Den Broeck, C., et al. 2009, *Classical and Quantum Gravity*, 26, 094021, doi: [10.1088/0264-9381/26/9/094021](https://doi.org/10.1088/0264-9381/26/9/094021)
- Auclair, P., Bacon, D., Baker, T., et al. 2023, *Living Reviews in Relativity*, 26, 5, doi: [10.1007/s41114-023-00045-2](https://doi.org/10.1007/s41114-023-00045-2)
- Babak, S., Gair, J. R., Petiteau, A., & Sesana, A. 2011, *Classical and Quantum Gravity*, 28, 114001, doi: [10.1088/0264-9381/28/11/114001](https://doi.org/10.1088/0264-9381/28/11/114001)
- Babak, S., Gair, J., Sesana, A., et al. 2017, *Phys. Rev. D*, 95, 103012, doi: [10.1103/PhysRevD.95.103012](https://doi.org/10.1103/PhysRevD.95.103012)
- Barack, L., & Cutler, C. 2004, *Phys. Rev. D*, 69, 082005, doi: [10.1103/PhysRevD.69.082005](https://doi.org/10.1103/PhysRevD.69.082005)
- Barausse, E. 2012, *Mon. Not. R. Astron. Soc.*, 423, 2533, doi: [10.1111/j.1365-2966.2012.21057.x](https://doi.org/10.1111/j.1365-2966.2012.21057.x)
- Bartos, I., Haiman, Z., Marka, Z., et al. 2017, *Nat. Commun.*, 8, 831, doi: [10.1038/s41467-017-00851-7](https://doi.org/10.1038/s41467-017-00851-7)
- Belgacem, E., Dirian, Y., Foffa, S., et al. 2019, *J. Cosmology Astropart. Phys.*, 2019, 015, doi: [10.1088/1475-7516/2019/08/015](https://doi.org/10.1088/1475-7516/2019/08/015)
- Berry, C. P. L., & Gair, J. R. 2013, *Mon. Not. R. Astron. Soc.*, 435, 3521, doi: [10.1093/mnras/stt1543](https://doi.org/10.1093/mnras/stt1543)
- Bonetti, M., & Sesana, A. 2020, *Phys. Rev. D*, 102, 103023, doi: [10.1103/PhysRevD.102.103023](https://doi.org/10.1103/PhysRevD.102.103023)
- Bonilla, A., Kumar, S., Nunes, R. C., & Pan, S. 2022, *Mon. Not. R. Astron. Soc.*, 512, 4231, doi: [10.1093/mnras/stac687](https://doi.org/10.1093/mnras/stac687)
- Borhanian, S., Dhani, A., Gupta, A., Arun, K. G., & Sathyaprakash, B. S. 2020, *Astrophys. J. Lett.*, 905, L28, doi: [10.3847/2041-8213/abcaf5](https://doi.org/10.3847/2041-8213/abcaf5)
- Braun, J., Dumm, J., De Palma, F., et al. 2008, *Astroparticle Physics*, 29, 299, doi: [10.1016/j.astropartphys.2008.02.007](https://doi.org/10.1016/j.astropartphys.2008.02.007)
- Burke, O., Gair, J. R., Simón, J., & Edwards, M. C. 2020, *Phys. Rev. D*, 102, 124054, doi: [10.1103/PhysRevD.102.124054](https://doi.org/10.1103/PhysRevD.102.124054)
- Bustamante, S., & Springel, V. 2019, *Mon. Not. R. Astron. Soc.*, 490, 4133, doi: [10.1093/mnras/stz2836](https://doi.org/10.1093/mnras/stz2836)
- Cai, R.-G., & Yang, T. 2017, *Phys. Rev. D*, 95, 044024, doi: [10.1103/PhysRevD.95.044024](https://doi.org/10.1103/PhysRevD.95.044024)
- Califano, M., de Martino, I., Vernieri, D., & Capozziello, S. 2023, *Phys. Rev. D*, 107, 123519, doi: [10.1103/PhysRevD.107.123519](https://doi.org/10.1103/PhysRevD.107.123519)
- Caprini, C., & Tamanini, N. 2016, *J. Cosmology Astropart. Phys.*, 2016, 006, doi: [10.1088/1475-7516/2016/10/006](https://doi.org/10.1088/1475-7516/2016/10/006)
- Chatterjee, S., Mondal, S., & Basu, P. 2023, *Mon. Not. R. Astron. Soc.*, 526, 5612, doi: [10.1093/mnras/stad3132](https://doi.org/10.1093/mnras/stad3132)
- Chen, H.-Y., Cowperthwaite, P. S., Metzger, B. D., & Berger, E. 2021, *Astrophys. J. Lett.*, 908, L4, doi: [10.3847/2041-8213/abdab0](https://doi.org/10.3847/2041-8213/abdab0)
- Chen, H.-Y., Fishbach, M., & Holz, D. E. 2018, *Nature*, 562, 545, doi: [10.1038/s41586-018-0606-0](https://doi.org/10.1038/s41586-018-0606-0)
- Chevallier, M., & Polarski, D. 2001, *International Journal of Modern Physics D*, 10, 213, doi: [10.1142/S0218271801000822](https://doi.org/10.1142/S0218271801000822)
- Chua, A. J. K., Katz, M. L., Warburton, N., & Hughes, S. A. 2021, *Phys. Rev. Lett.*, 126, 051102, doi: [10.1103/PhysRevLett.126.051102](https://doi.org/10.1103/PhysRevLett.126.051102)
- Chua, A. J. K., Moore, C. J., & Gair, J. R. 2017, *Phys. Rev. D*, 96, 044005, doi: [10.1103/PhysRevD.96.044005](https://doi.org/10.1103/PhysRevD.96.044005)
- Colpi, M., Danzmann, K., Hewitson, M., et al. 2024, arXiv e-prints, arXiv:2402.07571, doi: [10.48550/arXiv.2402.07571](https://doi.org/10.48550/arXiv.2402.07571)
- Croton, D. J., Stevens, A. R. H., Tonini, C., et al. 2016, *Astrophys. J. Suppl.*, 222, 22, doi: [10.3847/0067-0049/222/2/22](https://doi.org/10.3847/0067-0049/222/2/22)
- Cui, X.-Q., Zhao, Y.-H., Chu, Y.-Q., et al. 2012, *Research in Astronomy and Astrophysics*, 12, 1197, doi: [10.1088/1674-4527/12/9/003](https://doi.org/10.1088/1674-4527/12/9/003)
- Cusin, G., & Tamanini, N. 2021, *Mon. Not. R. Astron. Soc.*, 504, 3610, doi: [10.1093/mnras/stab1130](https://doi.org/10.1093/mnras/stab1130)
- Cutler, C., & Flanagan, É. E. 1994, *Phys. Rev. D*, 49, 2658, doi: [10.1103/PhysRevD.49.2658](https://doi.org/10.1103/PhysRevD.49.2658)
- Cutler, C., & Vallisneri, M. 2007, *Phys. Rev. D*, 76, 104018, doi: [10.1103/PhysRevD.76.104018](https://doi.org/10.1103/PhysRevD.76.104018)
- Dahlen, T., Mobasher, B., Somerville, R. S., et al. 2005, *Astrophys. J.*, 631, 126, doi: [10.1086/432027](https://doi.org/10.1086/432027)
- Dahlen, T., Mobasher, B., Faber, S. M., et al. 2013, *Astrophys. J.*, 775, 93, doi: [10.1088/0004-637X/775/2/93](https://doi.org/10.1088/0004-637X/775/2/93)
- Dalal, N., Holz, D. E., Hughes, S. A., & Jain, B. 2006, *Phys. Rev. D*, 74, 063006, doi: [10.1103/PhysRevD.74.063006](https://doi.org/10.1103/PhysRevD.74.063006)
- Dawson, K. S., Schlegel, D. J., Ahn, C. P., et al. 2013, *Astron. J.*, 145, 10, doi: [10.1088/0004-6256/145/1/10](https://doi.org/10.1088/0004-6256/145/1/10)

- Del Pozzo, W. 2012, *Phys. Rev. D*, 86, 043011, doi: [10.1103/PhysRevD.86.043011](https://doi.org/10.1103/PhysRevD.86.043011)
- Del Pozzo, W., Li, T. G. F., & Messenger, C. 2017, *Phys. Rev. D*, 95, 043502, doi: [10.1103/PhysRevD.95.043502](https://doi.org/10.1103/PhysRevD.95.043502)
- Del Pozzo, W., Sesana, A., & Klein, A. 2018, *Mon. Not. R. Astron. Soc.*, 475, 3485, doi: [10.1093/mnras/sty057](https://doi.org/10.1093/mnras/sty057)
- Derdzinski, A., & Mayer, L. 2023, *Mon. Not. R. Astron. Soc.*, 521, 4522, doi: [10.1093/mnras/stad749](https://doi.org/10.1093/mnras/stad749)
- Dhawan, S., Alsing, J., & Vagnozzi, S. 2021, *Mon. Not. R. Astron. Soc.*, 506, L1, doi: [10.1093/mnras/lsab058](https://doi.org/10.1093/mnras/lsab058)
- Di Valentino, E., Mena, O., Pan, S., et al. 2021, *Classical and Quantum Gravity*, 38, 153001, doi: [10.1088/1361-6382/ac086d](https://doi.org/10.1088/1361-6382/ac086d)
- Duras, F., Bongiorno, A., Ricci, F., et al. 2020, *Astron. Astrophys.*, 636, A73, doi: [10.1051/0004-6361/201936817](https://doi.org/10.1051/0004-6361/201936817)
- Fan, H.-M., Hu, Y.-M., Barausse, E., et al. 2020, *Phys. Rev. D*, 102, 063016, doi: [10.1103/PhysRevD.102.063016](https://doi.org/10.1103/PhysRevD.102.063016)
- Fan, H.-M., Zhong, S., Liang, Z.-C., et al. 2022, *Phys. Rev. D*, 106, 124028, doi: [10.1103/PhysRevD.106.124028](https://doi.org/10.1103/PhysRevD.106.124028)
- Feeney, S. M., Peiris, H. V., Williamson, A. R., et al. 2019, *Phys. Rev. Lett.*, 122, 061105, doi: [10.1103/PhysRevLett.122.061105](https://doi.org/10.1103/PhysRevLett.122.061105)
- Ferrarese, L., & Merritt, D. 2000, *Astrophys. J. Lett.*, 539, L9, doi: [10.1086/312838](https://doi.org/10.1086/312838)
- Finke, A., Foffa, S., Iacovelli, F., Maggiore, M., & Mancarella, M. 2021, *J. Cosmology Astropart. Phys.*, 2021, 026, doi: [10.1088/1475-7516/2021/08/026](https://doi.org/10.1088/1475-7516/2021/08/026)
- Finn, L. S. 1992, *Phys. Rev. D*, 46, 5236, doi: [10.1103/PhysRevD.46.5236](https://doi.org/10.1103/PhysRevD.46.5236)
- Fishbach, M., Gray, R., Magaña Hernandez, I., et al. 2019, *Astrophys. J. Lett.*, 871, L13, doi: [10.3847/2041-8213/aaf96e](https://doi.org/10.3847/2041-8213/aaf96e)
- Fishbach, M., & Holz, D. E. 2017, *Astrophys. J. Lett.*, 851, L25, doi: [10.3847/2041-8213/aa9bf6](https://doi.org/10.3847/2041-8213/aa9bf6)
- Fishbach, M., Doctor, Z., Callister, T., et al. 2021, *Astrophys. J.*, 912, 98, doi: [10.3847/1538-4357/abee11](https://doi.org/10.3847/1538-4357/abee11)
- Foreman-Mackey, D. 2016, *The Journal of Open Source Software*, 1, 24, doi: [10.21105/joss.00024](https://doi.org/10.21105/joss.00024)
- Foreman-Mackey, D., Hogg, D. W., Lang, D., & Goodman, J. 2013, *Publ. Astron. Soc. Pac.*, 125, 306, doi: [10.1086/670067](https://doi.org/10.1086/670067)
- Foreman-Mackey, D., Farr, W., Sinha, M., et al. 2019, *The Journal of Open Source Software*, 4, 1864, doi: [10.21105/joss.01864](https://doi.org/10.21105/joss.01864)
- Freedman, W. L. 2017, *Nature Astronomy*, 1, 0121, doi: [10.1038/s41550-017-0121](https://doi.org/10.1038/s41550-017-0121)
- Gallo, E., & Sesana, A. 2019, *Astrophys. J. Lett.*, 883, L18, doi: [10.3847/2041-8213/ab40c6](https://doi.org/10.3847/2041-8213/ab40c6)
- Gong, Y., Luo, J., & Wang, B. 2021, *Nature Astronomy*, 5, 881, doi: [10.1038/s41550-021-01480-3](https://doi.org/10.1038/s41550-021-01480-3)
- Gong, Y., Liu, X., Cao, Y., et al. 2019, *Astrophys. J.*, 883, 203, doi: [10.3847/1538-4357/ab391e](https://doi.org/10.3847/1538-4357/ab391e)
- Gray, R., Hernandez, I. M., Qi, H., et al. 2020, *Phys. Rev. D*, 101, 122001, doi: [10.1103/PhysRevD.101.122001](https://doi.org/10.1103/PhysRevD.101.122001)
- Greene, J. E., & Ho, L. C. 2007, *Astrophys. J.*, 667, 131, doi: [10.1086/520497](https://doi.org/10.1086/520497)
- Gupta, I. 2023, *Mon. Not. R. Astron. Soc.*, 524, 3537, doi: [10.1093/mnras/stad2115](https://doi.org/10.1093/mnras/stad2115)
- Han, W.-B., Zhong, X.-Y., Chen, X., & Xin, S. 2020, *Mon. Not. R. Astron. Soc.*, 498, L61, doi: [10.1093/mnras/lsaa115](https://doi.org/10.1093/mnras/lsaa115)
- He, W., Akiyama, M., Enoki, M., et al. 2024, *Astrophys. J.*, 962, 152, doi: [10.3847/1538-4357/ad1518](https://doi.org/10.3847/1538-4357/ad1518)
- Hirata, C. M., Holz, D. E., & Cutler, C. 2010, *Phys. Rev. D*, 81, 124046, doi: [10.1103/PhysRevD.81.124046](https://doi.org/10.1103/PhysRevD.81.124046)
- Holz, D. E., & Hughes, S. A. 2005, *Astrophys. J.*, 629, 15, doi: [10.1086/431341](https://doi.org/10.1086/431341)
- Hopkins, P. F., Richards, G. T., & Hernquist, L. 2007, *Astrophys. J.*, 654, 731, doi: [10.1086/509629](https://doi.org/10.1086/509629)
- Hopman, C., & Alexander, T. 2005, *Astrophys. J.*, 629, 362, doi: [10.1086/431475](https://doi.org/10.1086/431475)
- Hopman, C., Freitag, M., & Larson, S. L. 2007, *Mon. Not. R. Astron. Soc.*, 378, 129, doi: [10.1111/j.1365-2966.2007.11758.x](https://doi.org/10.1111/j.1365-2966.2007.11758.x)
- Hotokezaka, K., Nakar, E., Gottlieb, O., et al. 2019, *Nature Astronomy*, 3, 940, doi: [10.1038/s41550-019-0820-1](https://doi.org/10.1038/s41550-019-0820-1)
- Hu, W.-R., & Wu, Y.-L. 2017, *Natl. Sci. Rev.*, 4, 685, doi: [10.1093/nsr/nwx116](https://doi.org/10.1093/nsr/nwx116)
- Huang, S., Jiang, N., Zhu, J., et al. 2024, *arXiv e-prints*, arXiv:2403.01686, doi: [10.48550/arXiv.2403.01686](https://doi.org/10.48550/arXiv.2403.01686)
- Hughes, S. A., Warburton, N., Khanna, G., Chua, A. J. K., & Katz, M. L. 2021, *Phys. Rev. D*, 103, 104014, doi: [10.1103/PhysRevD.103.104014](https://doi.org/10.1103/PhysRevD.103.104014)
- Hunter, J. D. 2007, *Computing in Science and Engineering*, 9, 90, doi: [10.1109/MCSE.2007.55](https://doi.org/10.1109/MCSE.2007.55)
- Isoyama, S., Fujita, R., Chua, A. J. K., et al. 2022, *Phys. Rev. Lett.*, 128, 231101, doi: [10.1103/PhysRevLett.128.231101](https://doi.org/10.1103/PhysRevLett.128.231101)
- Ivezić, Ž., Kahn, S. M., Tyson, J. A., et al. 2019, *Astrophys. J.*, 873, 111, doi: [10.3847/1538-4357/ab042c](https://doi.org/10.3847/1538-4357/ab042c)
- Janssen, G., Hobbs, G., McLaughlin, M., et al. 2015, in *Advancing Astrophysics with the Square Kilometre Array (AASKA14)*, 37, doi: [10.22323/1.215.0037](https://doi.org/10.22323/1.215.0037)
- Jiang, Y.-F., Greene, J. E., & Ho, L. C. 2011, *Astrophys. J. Lett.*, 737, L45, doi: [10.1088/2041-8205/737/2/L45](https://doi.org/10.1088/2041-8205/737/2/L45)
- Jin, S.-J., He, D.-Z., Xu, Y., Zhang, J.-F., & Zhang, X. 2020, *J. Cosmology Astropart. Phys.*, 2020, 051, doi: [10.1088/1475-7516/2020/03/051](https://doi.org/10.1088/1475-7516/2020/03/051)

- Jin, S.-J., Zhang, Y.-Z., Song, J.-Y., Zhang, J.-F., & Zhang, X. 2023, *Science China Physics, Mechanics, and Astronomy*, 67, 220412, doi: [10.1007/s11433-023-2276-1](https://doi.org/10.1007/s11433-023-2276-1)
- Klein, A., Barausse, E., Sesana, A., et al. 2016, *Phys. Rev. D*, 93, 024003, doi: [10.1103/PhysRevD.93.024003](https://doi.org/10.1103/PhysRevD.93.024003)
- Klypin, A., Yepes, G., Gottlöber, S., Prada, F., & Heß, S. 2016, *Mon. Not. R. Astron. Soc.*, 457, 4340, doi: [10.1093/mnras/stw248](https://doi.org/10.1093/mnras/stw248)
- Kocsis, B., Frei, Z., Haiman, Z., & Menou, K. 2006, *Astrophys. J.*, 637, 27, doi: [10.1086/498236](https://doi.org/10.1086/498236)
- Kormendy, J., & Ho, L. C. 2013, *Annu. Rev. Astron. Astrophys.*, 51, 511, doi: [10.1146/annurev-astro-082708-101811](https://doi.org/10.1146/annurev-astro-082708-101811)
- Kyutoku, K., & Seto, N. 2016, *Mon. Not. R. Astron. Soc.*, 462, 2177, doi: [10.1093/mnras/stw1767](https://doi.org/10.1093/mnras/stw1767)
- Laghi, D., Tamanini, N., Del Pozzo, W., et al. 2021, *Mon. Not. R. Astron. Soc.*, 508, 4512, doi: [10.1093/mnras/stab2741](https://doi.org/10.1093/mnras/stab2741)
- Leandro, H., Marra, V., & Sturani, R. 2022, *Phys. Rev. D*, 105, 023523, doi: [10.1103/PhysRevD.105.023523](https://doi.org/10.1103/PhysRevD.105.023523)
- Levin, Y. 2003, arXiv e-prints, astro, doi: [10.48550/arXiv.astro-ph/0307084](https://doi.org/10.48550/arXiv.astro-ph/0307084)
- . 2007, *Mon. Not. R. Astron. Soc.*, 374, 515, doi: [10.1111/j.1365-2966.2006.11155.x](https://doi.org/10.1111/j.1365-2966.2006.11155.x)
- Lewis, A. 2019, arXiv e-prints, arXiv:1910.13970, doi: [10.48550/arXiv.1910.13970](https://doi.org/10.48550/arXiv.1910.13970)
- Li, R.-N., Zhao, Z.-Y., Gao, Z., & Wang, F.-Y. 2023, *Astrophys. J. Lett.*, 956, L2, doi: [10.3847/2041-8213/acfa9e](https://doi.org/10.3847/2041-8213/acfa9e)
- Liang, Z.-C., Hu, Y.-M., Jiang, Y., et al. 2022, *Phys. Rev. D*, 105, 022001, doi: [10.1103/PhysRevD.105.022001](https://doi.org/10.1103/PhysRevD.105.022001)
- Linder, E. V. 2003, *Phys. Rev. Lett.*, 90, 091301, doi: [10.1103/PhysRevLett.90.091301](https://doi.org/10.1103/PhysRevLett.90.091301)
- Liu, C., Laghi, D., & Tamanini, N. 2023, arXiv e-prints, arXiv:2310.12813, doi: [10.48550/arXiv.2310.12813](https://doi.org/10.48550/arXiv.2310.12813)
- Liu, S., Hu, Y.-M., Zhang, J.-d., & Mei, J. 2020, *Phys. Rev. D*, 101, 103027, doi: [10.1103/PhysRevD.101.103027](https://doi.org/10.1103/PhysRevD.101.103027)
- Luo, J., Chen, L.-S., Duan, H.-Z., et al. 2016, *Classical and Quantum Gravity*, 33, 035010, doi: [10.1088/0264-9381/33/3/035010](https://doi.org/10.1088/0264-9381/33/3/035010)
- MacLeod, C. L., & Hogan, C. J. 2008, *Phys. Rev. D*, 77, 043512, doi: [10.1103/PhysRevD.77.043512](https://doi.org/10.1103/PhysRevD.77.043512)
- Mandel, I., Farr, W. M., & Gair, J. R. 2019, *Mon. Not. R. Astron. Soc.*, 486, 1086, doi: [10.1093/mnras/stz896](https://doi.org/10.1093/mnras/stz896)
- Marchesini, D., van Dokkum, P., Quadri, R., et al. 2007, *Astrophys. J.*, 656, 42, doi: [10.1086/510305](https://doi.org/10.1086/510305)
- Marković, D. 1993, *Phys. Rev. D*, 48, 4738, doi: [10.1103/PhysRevD.48.4738](https://doi.org/10.1103/PhysRevD.48.4738)
- Mazzolari, G., Bonetti, M., Sesana, A., et al. 2022, *Mon. Not. R. Astron. Soc.*, 516, 1959, doi: [10.1093/mnras/stac2255](https://doi.org/10.1093/mnras/stac2255)
- McGee, S., Sesana, A., & Vecchio, A. 2020, *Nature Astronomy*, 4, 26, doi: [10.1038/s41550-019-0969-7](https://doi.org/10.1038/s41550-019-0969-7)
- Mei, J., Bai, Y.-Z., Bao, J., et al. 2021, *Progress of Theoretical and Experimental Physics*, 2021, 05A107, doi: [10.1093/ptep/ptaa114](https://doi.org/10.1093/ptep/ptaa114)
- Mikóczy, B., Kocsis, B., Forgács, P., & Vasúth, M. 2012, *Phys. Rev. D*, 86, 104027, doi: [10.1103/PhysRevD.86.104027](https://doi.org/10.1103/PhysRevD.86.104027)
- Miller, M. C., Freitag, M., Hamilton, D. P., & Lauburg, V. M. 2005, *Astrophys. J. Lett.*, 631, L117, doi: [10.1086/497335](https://doi.org/10.1086/497335)
- Muttoni, N., Mangiagli, A., Sesana, A., et al. 2022, *Phys. Rev. D*, 105, 043509, doi: [10.1103/PhysRevD.105.043509](https://doi.org/10.1103/PhysRevD.105.043509)
- Nan, R., Li, D., Jin, C., et al. 2011, *International Journal of Modern Physics D*, 20, 989, doi: [10.1142/S0218271811019335](https://doi.org/10.1142/S0218271811019335)
- Nandra, K., Barret, D., Barcons, X., et al. 2013, arXiv e-prints, arXiv:1306.2307, doi: [10.48550/arXiv.1306.2307](https://doi.org/10.48550/arXiv.1306.2307)
- Naoz, S., & Haiman, Z. 2023, *Astrophys. J. Lett.*, 955, L27, doi: [10.3847/2041-8213/acf8c9](https://doi.org/10.3847/2041-8213/acf8c9)
- Naoz, S., Rose, S. C., Michaely, E., et al. 2022, *Astrophys. J. Lett.*, 927, L18, doi: [10.3847/2041-8213/ac574b](https://doi.org/10.3847/2041-8213/ac574b)
- Nissanke, S., Holz, D. E., Dalal, N., et al. 2013, arXiv e-prints, arXiv:1307.2638, doi: [10.48550/arXiv.1307.2638](https://doi.org/10.48550/arXiv.1307.2638)
- Palmese, A., deVicente, J., Pereira, M. E. S., et al. 2020, *Astrophys. J. Lett.*, 900, L33, doi: [10.3847/2041-8213/abaeff](https://doi.org/10.3847/2041-8213/abaeff)
- Pan, Z., Lyu, Z., & Yang, H. 2021, *Phys. Rev. D*, 104, 063007, doi: [10.1103/PhysRevD.104.063007](https://doi.org/10.1103/PhysRevD.104.063007)
- . 2022, *Phys. Rev. D*, 105, 083005, doi: [10.1103/PhysRevD.105.083005](https://doi.org/10.1103/PhysRevD.105.083005)
- Pan, Z., & Yang, H. 2021, *Phys. Rev. D*, 103, 103018, doi: [10.1103/PhysRevD.103.103018](https://doi.org/10.1103/PhysRevD.103.103018)
- Perivolaropoulos, L., & Skara, F. 2022, *New Astron. Rev.*, 95, 101659, doi: [10.1016/j.newar.2022.101659](https://doi.org/10.1016/j.newar.2022.101659)
- Petiteau, A., Babak, S., & Sesana, A. 2011, *Astrophys. J.*, 732, 82, doi: [10.1088/0004-637X/732/2/82](https://doi.org/10.1088/0004-637X/732/2/82)
- Punturo, M., Abernathy, M., Acernese, F., et al. 2010, *Classical and Quantum Gravity*, 27, 194002, doi: [10.1088/0264-9381/27/19/194002](https://doi.org/10.1088/0264-9381/27/19/194002)
- Reardon, D. J., Zic, A., Shannon, R. M., et al. 2023, *Astrophys. J. Lett.*, 951, L6, doi: [10.3847/2041-8213/acdd02](https://doi.org/10.3847/2041-8213/acdd02)
- Reitze, D., Adhikari, R. X., Ballmer, S., et al. 2019, in *Bulletin of the American Astronomical Society*, Vol. 51, 35, doi: [10.48550/arXiv.1907.04833](https://doi.org/10.48550/arXiv.1907.04833)

- Riess, A. G., Casertano, S., Yuan, W., et al. 2021, *Astrophys. J. Lett.*, 908, L6, doi: [10.3847/2041-8213/abdbaf](https://doi.org/10.3847/2041-8213/abdbaf)
- Ruan, W.-H., Liu, C., Guo, Z.-K., Wu, Y.-L., & Cai, R.-G. 2020, *Nature Astronomy*, 4, 108, doi: [10.1038/s41550-019-1008-4](https://doi.org/10.1038/s41550-019-1008-4)
- Rubbo, L. J., Holley-Bockelmann, K., & Finn, L. S. 2006, in *American Institute of Physics Conference Series*, Vol. 873, *Laser Interferometer Space Antenna: 6th International LISA Symposium*, ed. S. M. Merkowitz & J. C. Livas (AIP), 284–288, doi: [10.1063/1.2405057](https://doi.org/10.1063/1.2405057)
- Sathyaprakash, B. S., & Schutz, B. F. 2009, *Living Rev. Rel.*, 12, 2, doi: [10.12942/lrr-2009-2](https://doi.org/10.12942/lrr-2009-2)
- Scaramella, R., Amiaux, J., Mellier, Y., et al. 2022, *Astron. Astrophys.*, 662, A112, doi: [10.1051/0004-6361/202141938](https://doi.org/10.1051/0004-6361/202141938)
- Schechter, P. 1976, *Astrophys. J.*, 203, 297, doi: [10.1086/154079](https://doi.org/10.1086/154079)
- Schutz, B. F. 1986, *Nature*, 323, 310, doi: [10.1038/323310a0](https://doi.org/10.1038/323310a0)
- Scott, N., & Graham, A. W. 2013, *Astrophys. J.*, 763, 76, doi: [10.1088/0004-637X/763/2/76](https://doi.org/10.1088/0004-637X/763/2/76)
- Sesana, A. 2016, *Phys. Rev. Lett.*, 116, 231102, doi: [10.1103/PhysRevLett.116.231102](https://doi.org/10.1103/PhysRevLett.116.231102)
- Sesana, A., Barausse, E., Dotti, M., & Rossi, E. M. 2014, *Astrophys. J.*, 794, 104, doi: [10.1088/0004-637X/794/2/104](https://doi.org/10.1088/0004-637X/794/2/104)
- Sisk-Reynés, J., Reynolds, C. S., Matthews, J. H., & Smith, R. N. 2022, *Mon. Not. R. Astron. Soc.*, 514, 2568, doi: [10.1093/mnras/stac1389](https://doi.org/10.1093/mnras/stac1389)
- Soares-Santos, M., Palmese, A., Hartley, W., et al. 2019, *Astrophys. J. Lett.*, 876, L7, doi: [10.3847/2041-8213/ab14f1](https://doi.org/10.3847/2041-8213/ab14f1)
- Song, J.-Y., Wang, L.-F., Li, Y., et al. 2022, arXiv e-prints, arXiv:2212.00531, doi: [10.48550/arXiv.2212.00531](https://doi.org/10.48550/arXiv.2212.00531)
- Tagawa, H., Haiman, Z., & Kocsis, B. 2020, *Astrophys. J.*, 898, 25, doi: [10.3847/1538-4357/ab9b8c](https://doi.org/10.3847/1538-4357/ab9b8c)
- Tamanini, N., Caprini, C., Barausse, E., et al. 2016, *J. Cosmology Astropart. Phys.*, 2016, 002, doi: [10.1088/1475-7516/2016/04/002](https://doi.org/10.1088/1475-7516/2016/04/002)
- Taylor, S. R., Gair, J. R., & Mandel, I. 2012, *Phys. Rev. D*, 85, 023535, doi: [10.1103/PhysRevD.85.023535](https://doi.org/10.1103/PhysRevD.85.023535)
- Torres-Orjuela, A., Amaro Seoane, P., Xuan, Z., et al. 2021, *Phys. Rev. Lett.*, 127, 041102, doi: [10.1103/PhysRevLett.127.041102](https://doi.org/10.1103/PhysRevLett.127.041102)
- Vallisneri, M. 2008, *Phys. Rev. D*, 77, 042001, doi: [10.1103/PhysRevD.77.042001](https://doi.org/10.1103/PhysRevD.77.042001)
- van der Walt, S., Colbert, S. C., & Varoquaux, G. 2011, *Computing in Science and Engineering*, 13, 22, doi: [10.1109/MCSE.2011.37](https://doi.org/10.1109/MCSE.2011.37)
- Vasylyev, S. S., & Filippenko, A. V. 2020, *Astrophys. J.*, 902, 149, doi: [10.3847/1538-4357/abb5f9](https://doi.org/10.3847/1538-4357/abb5f9)
- Veronesi, N., Rossi, E. M., & van Velzen, S. 2023, *Mon. Not. R. Astron. Soc.*, 526, 6031, doi: [10.1093/mnras/stad3157](https://doi.org/10.1093/mnras/stad3157)
- Veronesi, N., Rossi, E. M., van Velzen, S., & Buscicchio, R. 2022, *Mon. Not. R. Astron. Soc.*, 514, 2092, doi: [10.1093/mnras/stac1346](https://doi.org/10.1093/mnras/stac1346)
- Virtanen, P., Gommers, R., Oliphant, T. E., et al. 2020, *Nature Methods*, 17, 261, doi: [10.1038/s41592-019-0686-2](https://doi.org/10.1038/s41592-019-0686-2)
- Wang, H., & Giannios, D. 2021, *Astrophys. J.*, 908, 200, doi: [10.3847/1538-4357/abd39c](https://doi.org/10.3847/1538-4357/abd39c)
- Wang, H.-T., Jiang, Z., Sesana, A., et al. 2019a, *Phys. Rev. D*, 100, 043003, doi: [10.1103/PhysRevD.100.043003](https://doi.org/10.1103/PhysRevD.100.043003)
- Wang, L.-F., Jin, S.-J., Zhang, J.-F., & Zhang, X. 2022a, *Science China Physics, Mechanics, and Astronomy*, 65, 210411, doi: [10.1007/s11433-021-1736-6](https://doi.org/10.1007/s11433-021-1736-6)
- Wang, M., Yin, J., Ma, Y., & Wu, Q. 2022b, *Astrophys. J.*, 933, 225, doi: [10.3847/1538-4357/ac75e6](https://doi.org/10.3847/1538-4357/ac75e6)
- Wang, R., Ruan, W.-H., Yang, Q., et al. 2022, *Natl. Sci. Rev.*, 9, nwab054, doi: [10.1093/nsr/nwab054](https://doi.org/10.1093/nsr/nwab054)
- Wang, T., Liu, G., Cai, Z., et al. 2023, *Science China Physics, Mechanics, and Astronomy*, 66, 109512, doi: [10.1007/s11433-023-2197-5](https://doi.org/10.1007/s11433-023-2197-5)
- Wang, Y. Y., Wang, F. Y., Zou, Y. C., & Dai, Z. G. 2019b, *Astrophys. J. Lett.*, 886, L22, doi: [10.3847/2041-8213/ab55e2](https://doi.org/10.3847/2041-8213/ab55e2)
- Waskom, M. L. 2021, *Journal of Open Source Software*, 6, 3021, doi: [10.21105/joss.03021](https://doi.org/10.21105/joss.03021)
- Wu, Z., Fan, H.-M., Hu, Y.-M., & Heng, I. S. 2023, arXiv e-prints, arXiv:2308.15354, doi: [10.48550/arXiv.2308.15354](https://doi.org/10.48550/arXiv.2308.15354)
- Xu, H., Chen, S., Guo, Y., et al. 2023, *Research in Astronomy and Astrophysics*, 23, 075024, doi: [10.1088/1674-4527/acdfa5](https://doi.org/10.1088/1674-4527/acdfa5)
- Xuan, Z., Naoz, S., & Chen, X. 2023, *Phys. Rev. D*, 107, 043009, doi: [10.1103/PhysRevD.107.043009](https://doi.org/10.1103/PhysRevD.107.043009)
- You, Z.-Q., Zhu, X.-J., Ashton, G., Thrane, E., & Zhu, Z.-H. 2021, *Astrophys. J.*, 908, 215, doi: [10.3847/1538-4357/abd4d4](https://doi.org/10.3847/1538-4357/abd4d4)
- Yu, J., Wang, Y., Zhao, W., & Lu, Y. 2020, *Mon. Not. R. Astron. Soc.*, 498, 1786, doi: [10.1093/mnras/staa2465](https://doi.org/10.1093/mnras/staa2465)
- Yuan, W., Zhang, C., Feng, H., et al. 2015, arXiv e-prints, arXiv:1506.07735, doi: [10.48550/arXiv.1506.07735](https://doi.org/10.48550/arXiv.1506.07735)
- Yuan, X., Li, Z., Liu, X., et al. 2020, in *Society of Photo-Optical Instrumentation Engineers (SPIE) Conference Series*, Vol. 11445, *Ground-based and Airborne Telescopes VIII*, ed. H. K. Marshall, J. Spyromilio, & T. Usuda, 114457M, doi: [10.1117/12.2562334](https://doi.org/10.1117/12.2562334)

- Yunes, N., Kocsis, B., Loeb, A., & Haiman, Z. 2011, *Phys. Rev. Lett.*, 107, 171103,
doi: [10.1103/PhysRevLett.107.171103](https://doi.org/10.1103/PhysRevLett.107.171103)
- Yunes, N., Sopuerta, C. F., Rubbo, L. J., & Holley-Bockelmann, K. 2008, *Astrophys. J.*, 675, 604,
doi: [10.1086/525839](https://doi.org/10.1086/525839)
- Zhao, W., & Wen, L. 2018, *Phys. Rev. D*, 97, 064031,
doi: [10.1103/PhysRevD.97.064031](https://doi.org/10.1103/PhysRevD.97.064031)
- Zhou, X., Gong, Y., Meng, X.-M., et al. 2021, *Astrophys. J.*, 909, 53, doi: [10.3847/1538-4357/abda3e](https://doi.org/10.3847/1538-4357/abda3e)
- . 2022, *Mon. Not. R. Astron. Soc.*, 512, 4593,
doi: [10.1093/mnras/stac786](https://doi.org/10.1093/mnras/stac786)
- Zhu, L.-G., & Chen, X. 2023, *Astrophys. J.*, 948, 26,
doi: [10.3847/1538-4357/acc24b](https://doi.org/10.3847/1538-4357/acc24b)
- . 2024, *Astrophys. J.*, 960, 43,
doi: [10.3847/1538-4357/ad0cf2](https://doi.org/10.3847/1538-4357/ad0cf2)
- Zhu, L.-G., Hu, Y.-M., Wang, H.-T., et al. 2022a, *Phys. Rev. Res.*, 4, 013247,
doi: [10.1103/PhysRevResearch.4.013247](https://doi.org/10.1103/PhysRevResearch.4.013247)
- Zhu, L.-G., Xie, L.-H., Hu, Y.-M., et al. 2022b, *Science China Physics, Mechanics, and Astronomy*, 65, 259811,
doi: [10.1007/s11433-021-1859-9](https://doi.org/10.1007/s11433-021-1859-9)